THESIS FOR THE DEGREE OF LICENTIATE OF ENGINEERING

Methane and Carbon Monoxide Oxidation over Pd and Pt

A Density Functional Theory and Microkinetic Study

Adriana Trinchero

Department of Applied Physics

CHALMERS UNIVERSITY OF TECHNOLOGY

Göteborg, Sweden 2013

Methane and Carbon Monoxide Oxidation over Pd and Pt
A Density Functional Theory and Microkinetic Study
Adriana Trinchero

Department of Applied Physics
Chalmers University of Technology
SE-412 96 Göteborg, Sweden
Telephone: +46 (0)31 772 1000

Printed by:
Chalmers Reproservice
Göteborg, Sweden 2013

Methane and Carbon Monoxide Oxidation over Pd and Pt
A Density Functional Theory and Microkinetic Study
Adriana Trinchero
Department of Applied Physics
Chalmers University of Technology, Göteborg 2013

Abstract

Efficient transportation is a key component in modern society. Transportation is, however, also a major source of air pollution which affects health as well as environment. This has led to strict legislations on emissions for the automotive sector and the development of catalytic techniques for emission control. In particular, the three way catalyst has improved the urban air quality. The environmental impact together with winding oil resources are the driving forces for improved energy efficiency and exploration of alternative fuels. A viable bridge between fossil fuels and renewable energy sources is natural gas. The main component of natural gas is methane, yielding the most amount of energy per mole of formed CO_2 of all hydrocarbons. The two most common metals used in catalytic converters for methane oxidation are Pd and Pt.

In spite of many studies, the mechanisms for compete oxidation of methane are still under debate. The reason is the inherent complexity of heterogeneous catalysis, where different time and length scales affect the measured catalytic reaction rate. The purpose of this study is to combine electronic structure calculations with microkinetic modeling in order to bridge time end length scales. The study shows that methane oxidation, in principle, is structure sensitive, but that smaller particles not necessarily will increase the rate of the reaction.

Carbon monoxide is relevant both as an intermediate in methane oxidation and as the reason for to the cold start problem; at low temperatures, carbon monoxide poisons the catalyst and hinders any reactions to occur. Furthermore, the oxidation of carbon monoxide exhibits several interesting reaction kinetic phenomena such as bi-stability oscillations and standing waves. The results in this study show that the reaction is highly structure sensitivity and several reaction parameters affect the activity, including sticking coefficients and activation barriers. For CO oxidation, the measured activity is found to be directly correlated to the energy barrier of the rate determining step.

Keywords: **methane, carbon monoxide, oxidation, Pd, Pt, heterogeneous catalysis, DFT, microkinetic modeling.**

List of Publications

This thesis is based on the work presented in the following publications, referred to by Roman numerals (**I-II**) in the text:

I. Local catalytic ignition during CO oxidation on low-index Pt and Pd surfaces: A combined PEEM, MS and DFT study.
D. Vogel, C. Spiel, Y. Suchorski, A. Trinchero, R. Schögl, H. Grönbeck and G. Rupprechter
Angewandte Chemie International Edition, **51** (2012) 10041.

II. Methane oxidation over Pd and Pt studied by DFT and kinetic modeling
A. Trinchero, A. Hellman and H. Grönbeck
Surface Science (submitted).

Related publications not included in this thesis:

1. **The Active Phase of Palladium during Methane Oxidation**
A. Hellman, A. Resta, N. M. Martin, J. Gustafson, A. Trinchero, P. -A. Carlsson, O. Balmes, R. Felici, R. van Rijn, J. W. M. Frenken, J. N. Andersen, E. Lundgren, and H. Grönbeck
Physical Chemistry Letters, **2** (2012) 678.

My contributions to the publications

Paper I
I performed the DFT calculations.

Paper II
I performed all calculations and wrote the first draft of the paper.

Contents

Chapter 1

Introduction

Todays society is heavily dependent on transportation, it enables trade and movement of people within and between countries, and has a major impact on the social development and welfare. However, it has been realized that automotive transportation is a major source of air pollution, with tangible effects on health [1] and enviroment. Moreover, transportation is reliant on fossil fuels and consumes more than half of the oil production in the world [2]. These two problems, i) environmental impact and ii) winding oil resources are severe problems and currently the target of many scientific studies.

As a response to the detrimental effect on health [3, 4] and environment [3], caused by pollution from transportation-related sources, the Clean Air Act established in the 1970's, air-quality standards in USA for six major pollutants: particulate matter, sulfur oxides, carbon monoxide, nitrogen oxides, hydrocarbons and photochemical oxidants. The regulations of the amount of exhaust emissions from new vehicles, forced the automotive industry to develop emission control technology, e.g. the catalytic converter. Today, the California Air Resources Board (CARBS) sets new standards continuously, ultimately aiming towards zero emission vehicles [5].

The first catalytic converter was the two way catalyst, that treated uncombusted hydrocarbons and carbon monoxide. Later, the introduction of the three way catalyst (TWC) also addressed pollution caused by nitrous oxides. The TWC transforms hydrocarbons, carbon monoxide and NO_X into water, CO_2 and N_2

The active material in the catalytic converter is small metal nano-particles dispersed on a porous metaloxide that is coated onto a multichannel array called a monolith, where the exhaust gases pass trough. The metal nano-particles make up 1-2 % of the catalytic converter and lowers the activation energies for the

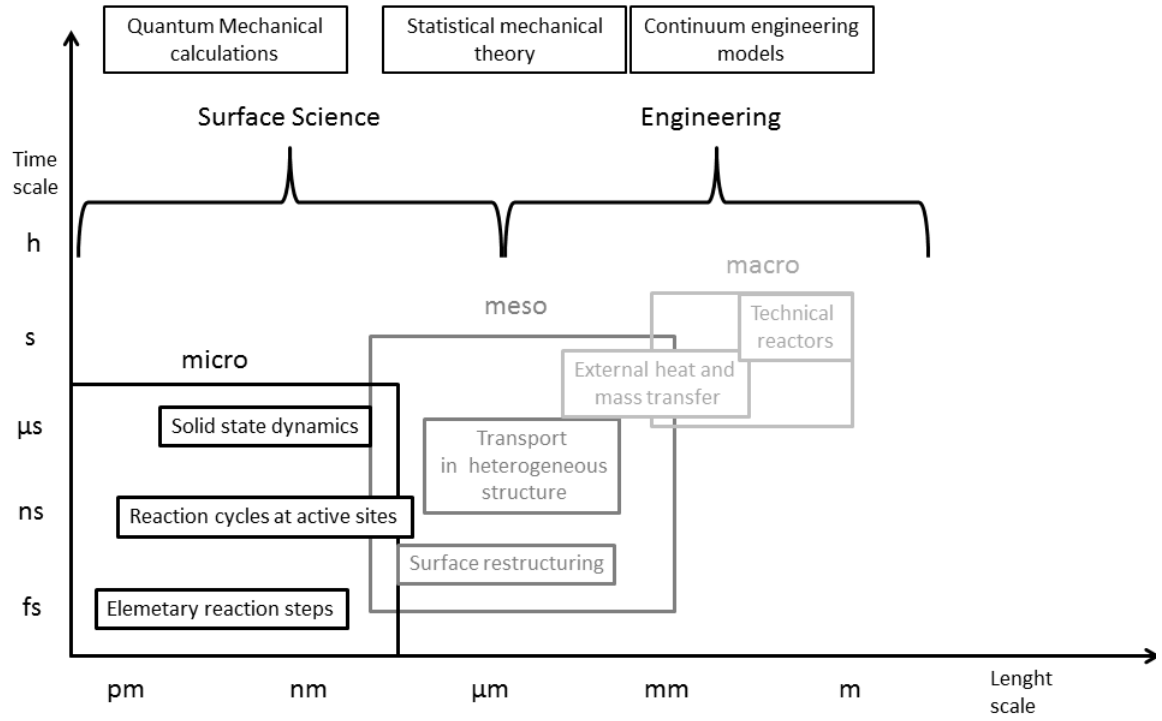

Figure 1.1: Schematic figure illustrating the different time and length scales important for catalysis. The possible computational modelling at each level are also shown. The figure is adapted from [14, 15].

reactions. Materials that facilitate reactions without being consumed are called catalysts. If reactants and catalyst are in different phases (in this case, solid- and gas-phase) the term heterogeneous catalysis is used.

Figure 1 shows the different time and length scales involved in heterogeneous catalysis. Processes at all scales are important to understand the measured rates at the applied, macro scale. However, it is on the surfaces of the nano-sized metal particles where the chemistry takes place, i.e. where bonds are broken and formed. This level provides atomistic understanding of elementary steps and rationalizes trends in reactivity. The meso level, where the statistical mechanical theory describes the relevant phenomena, is where the small nano-metal-particles, their shape and size (from 1-10 nanometers) and how their properties relate to their catalytic activity, are important. Furthermore, transport phenomena as diffusion into pores of the oxide support are relevant at this scale. The third level is related to the shape of the catalytic converter, with length scales varying from mm to

cm. Here, the porosity and the strength of the catalysis are important. The last level is the macroscopic one. There are also different time scales reflecting the different length scales, from the sub-picosecond regime where a bond is broken to the completion of the residence time of molecules inside the entire reactor.

Due to the complex structure of technical catalysts, with important phenomena occurring at different time and length scales, it is generally challenging to establish proper model systems. Many of the methods available for studying the catalysts at the atomic scale require low pressures, i.e. ultra high vacuum conditions. However, the most stable surface at low pressures is not necessarily the stable surface at real reaction conditions (at atmospheric pressures). Surfaces are known to be dynamic systems that respond to the environment [6, 7]. This gap between surface science conditions and conditions where technical catalyst are used is known as the pressure gap. The study of single crystals surfaces, which can be different than the actual surface in a catalyst, creates another problem known as the materials gap. At the surface science scale, is possible to gain understanding of the reactions and atomic scale events, when this information is translated to catalytic activity, there is a way to design new catalytic materials in a rational manner. There is continuous work to bridge the pressure and materials gaps. Ambient pressure x-ray photo emission spectrometry (AP-XPS) is one such technique developed and used to successfully study catalytic systems at high pressures [6]. Other examples are: in situ environmental transmission electron microscopy [8], scanning tunneling microscopy (STM) [9], in situ surface x-ray diffraction [10], in situ X-ray absorption near edge structure (XANES) spectroscopy studies to correlate changes in the surface of the catalyst with its activity [11]. Moreover, molecular beam experiments may allow investigations of the kinetic and dynamics of the surface reactions of supported catalytic particles [12, 13].

The focus of the present study is on the oxidation of methane and carbon monoxide for automotive applications. The interest in methane originates from the possibility to use natural gas as an intermediate solution to the dwindling oil resources. The oil reserves have been predicted to peak within ten years [16–18], whereas the resources of natural gas are predicted to last at least for 60 years [19]. The Natural Gas Vehicle (NGV) is already used around the world in countries such as Iran, Pakistan, Argentina and Brasil [20]. Methane is the cleanest of the fossil fuels, and the engine out emissions of NO_x and SO_x are below the current emissions standards [21]. A catalyst is needed in the NGV to ensure the complete oxidation of methane, so that no traces of methane or carbon monoxide reach the

atmosphere. This is important because methane has 10 times the CO_2 global warming potential (GWP) per mole [22]. The CO oxidation reaction is studied due to the cold start problem. At low temperatures carbon monoxide poisons the surface thereby hindering any reactions on the catalyst. This is a severe problem and accounts for the major part of emitted CO and hydrocarbons [5, 23]. Moreover, carbon monoxide is interesting as a model reaction. Extensive experimental [24–27] and theoretical [28–35] studies have shown that CO oxidation exhibits several interesting reaction kinetic phenomena such as oscillations and bi-stability.

1.1 Objectives

The aim of this report is to investigate the oxidation of methane and carbon monoxide in connection to automotive catalysis. This is done at an atomistic level using the density functional theory (DFT). The results are used in a microkinetic model to gain further insight of the reactivity and activity of the catalyst. Paper I is a collaboration between experiments and theory, whereas Paper II is a pure modeling study. The ambition of the papers have been to relate phenomena occurring at the atomic or micro scale with the measured catalytic activities.

Chapter 2

Reactions at metal surfaces

The focus of this chapter is on the structure of metal particles, the reactivity of the metal surfaces and how trends in reactivity can be be explained by simple models. Many of the concepts discussed here are available in books dedicated to catalysis, physical chemistry and material science [2, 36, 37].

2.1 Metal particles

For metal atoms in the bulk phase, the number of nearest neighbors (NN) for each atom is not equal to their valence (which is the case for other groups in the periodic table). Instead, the atoms have 12 (fcc-cubic, bcc cubic and hexagonal) or 8 (simple cubic) NN, implying that the number of valence electrons (per atom) is significantly less than the number of NNs. This means that the valence electrons do not enter well localized orbitals. Instead they are shared among all atoms, i.e. the orbitals are extended throughout the crystal and the bonding is non-directional. This is especially true for the sp-metals, for the transition metals, states originating from atomic d-states are more localized. Generally, the driving force for aggregation can be viewed as a delocalization phenomena. The delocalization of an electron over the solid lowers the electronic kinetic energy associated with its confinement [37], experienced by gas-phase atoms.

A finite metal particle has some atoms exposed to the surrounding environment. These exposed atoms have fewer NNs and are consequently uncoordinated. The Wulff construction is a method to determine the equilibrium shape of a crystalline particle [38]. The shape is given by energy minimization, which gives preference to certain crystal planes. The plane with lowest surface energy will dominate the crystal polyhedron. For close packed metals (as Pd and Pt) the sur-

face with lowest energy is the (111) facet because this facet has the most compact atomic arrangement.

A Wulff shaped Pd particle is shown in Figure 2.1. The particle exemplifies the surface planes investigated in the appended papers. The most abundant surface is the (111), followed by the (100) facet. The (211) facet appears in the intersection between (111) and (100). The corner site on the particle is modeled by the (321) site. Note that, although (110) has a lower surface energy that (100), geometrical restrictions make this surface abundant only in small amounts.

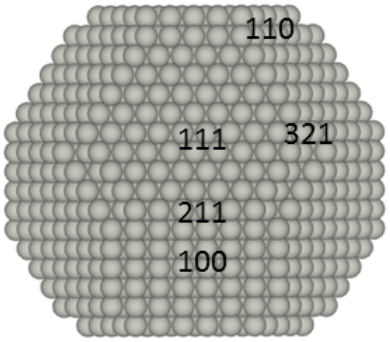

Figure 2.1: The Wulff shape for a ∼3 nm sized Pd particle. The (111), (110), (100), (211) and the corner site (321) facets are indicated. The particle has been generated with the experimental values for the surface energies (γ): $\gamma_{111} = 1.92\ Jm^{-2}$, $\gamma_{110} = 2.225\ Jm^{-2}$, $\gamma_{100} = 2.362\ Jm^{-2}$ [39].

In a technical catalyst, the metal particles are anchored to an oxide support, hence the shape of the Wulff particle will also depend on the energy of the interaction between the support and the crystallite. The adhesion energy (β) will determine how the particle is truncated and the degree of wetting. A schematic representation of the particle-support interaction is shown in Figure 2.2. For Pd on Al_2O_3, the interaction with the support is minimal [8].

There are other factors that affect the shape (and size) of a nanoparticle. One important factor is the environment. Phenomena such as surface reconstructions can be driven by the adsorbate coverage on the surface [25]. Moreover, the character of the environment, oxidative or reducing, can affect the preference of the exposed surfaces [6, 40]. Hence, the particle is a non-static system, that responds to the surrounding.

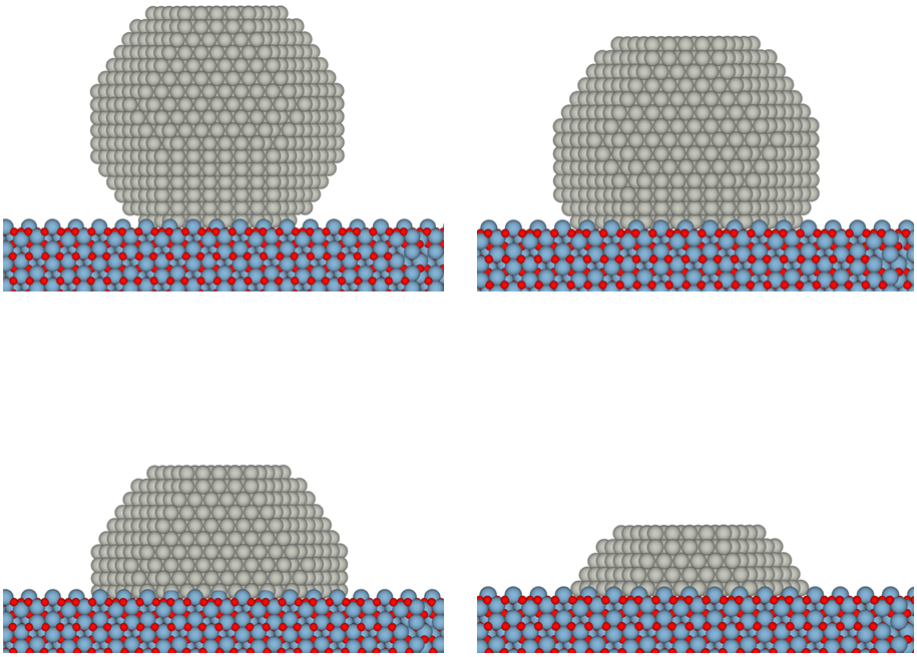

Figure 2.2: The Wulff shape for a ∼3 nm sized Pd particle on an oxide support with increased interface energy.

2.2 Physisorption and chemisorption

A molecule can interact with a surface in different ways. Figure 2.3 shows a schematic potential energy curve for a diatomic molecule over a hypothetical surface. At medium distances, the molecule physisorbs, at shorter distances the molecule chemisorbs either associatively or dissociatively. The preferred type of interaction depends on which interaction that renders the lowest energy. For O_2 adsorption on Pt(111), both associative and dissociative chemisorption are seen at different temperatures [41].

Physisorption lacks a true chemical bond, a good example of this is methane adsorbed onto metal surfaces. The physisorption well originates from weak dipole interactions, which depend on the polarizability of the adsorbate and the metal.

Chemisorption, on the other hand, implies the formation of chemical bonds. This is the case when CO binds to Palladium or Platinum surfaces. Furthermore, as compared to physisorption, the enthalpy of chemisorption is stronger. For methane, typical adsorption energies on the above mentioned metals are around 0.2 eV. For CO, the adsorption energies are instead close to 2 eV.

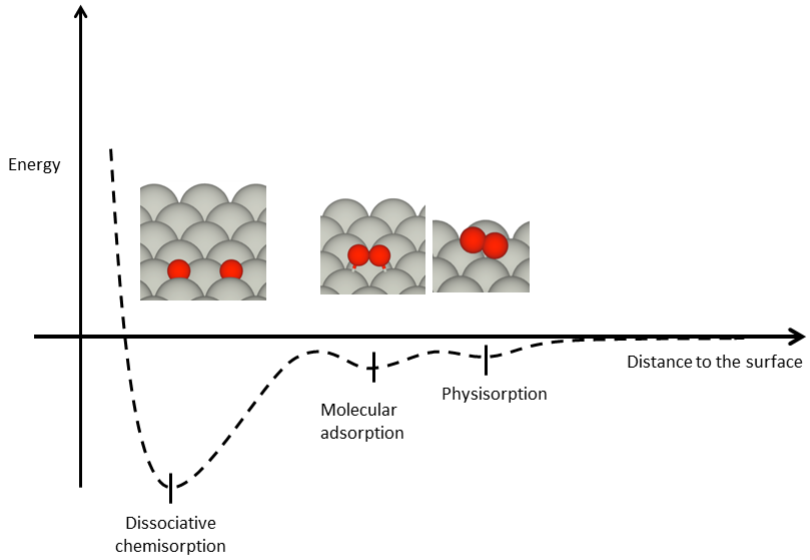

Figure 2.3: The interaction of a diatomic molecule at different distances from a metal surface. The atoms in red represent the di-atomic molecule and the grey atoms represent the surface atoms.

In some cases chemisorption causes a rupture of the molecular bond. This is called dissociative chemisorption as opposite to associative chemisorption, where all the bonds stay more or less intact upon adsorption. The same adsorbate may adsorb differently on different metals. Carbon monoxide adsorbs associatively on the metals to the right of the periodic table and dissociatively at the left. The boarder to where CO turns to adsorb dissociatively instead of associatively is between Fe-Co, Tc-Ru, and Re-Os [42].

2.3 Models for adsorption

Many features of chemisorption can be understood within the Newns-Anderson (N-A) model [43,44], which describes the interaction between an adsorbate and a metal surface and how it affects the electronic structure of the interacting systems. The model assumes that the electronic bands in the solid have an elliptic shape; the sp-bands being wide and the d-band being narrow. Here, only a summary of the results from the N-A model is presented. For a more mathematical description

I refer to [2].

Adsorption on a free-electron metal

Substantial overlap between neighboring sp-orbitals renders a wide band in the metal. As a consequence, free electron metals have broad bands. When the adsorbate approaches the metals states, the electronic levels of the adsorbate broadens and shift down in energy. The broader the band, the more stabilized is the adsorbate upon adsorption. This is shown schematically in Figure 2.4.

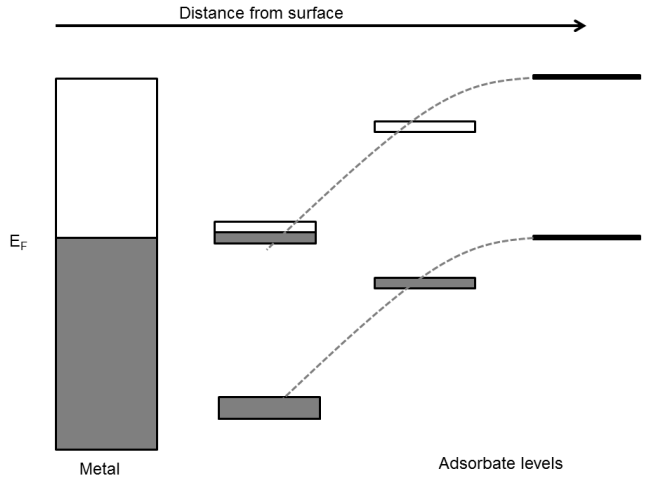

Figure 2.4: Schematic view of how the energy levels of an adsorbate are lowered and are broadened upon adsorption to a free-electron metal. The figure is adapted from [2].

Adsorption on a transition metal

The transition metal has in addition to a wide sp-band, a narrow d-band. The d-band interacts strongly with the adsorbate and leads to the splitting of its states to bonding and anti-bonding combinations. For a molecule such as H_2, both bonding and anti-bonding molecular orbitals contribute to the chemisorption bond (Figure 2.5). Filling the molecular antibonding orbital (here, σ^*), strengthens the interaction with the surface but weakens the intramolecular bond. This is important as it explains trends in the dissociative adsorption of H_2 on transition metals [45]. Such filling of the anti-bonding orbital in the molecule by the metal is called back-donation.

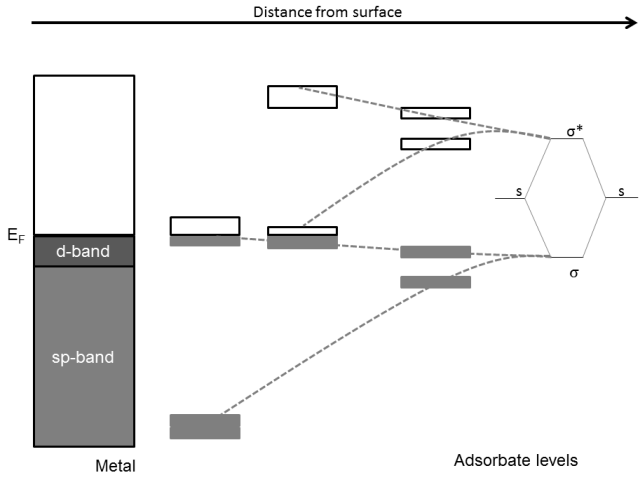

Figure 2.5: Schematic view of how the energy levels of an adsorbate are broadened by interaction with the sp-band. The interaction with the d-band result in a splitting of the bonding and anti-bonding orbitals in the molecule. The figure is adaptated from [2].

The d-band model

The d-band model [46, 47] has been used to explain trends in adsorption and reactivity. The model is a special case the of N-A model, and shows that trends in reactivity in many cases can be understood from the interaction between d-states and the molecular states that have been shifted due to the interaction with the sp-bands in the metal.

The bond mechanism of CO onto metal surfaces is generally discussed within the Blyholder model [48]. Upon adsorption the bonding 5σ states of CO donate charge to the surface and the surface back-donates to the anti-bonding $2\pi^*$ CO orbital. In Figure 2.6, a projected density of states is shown for CO on Al(111) and Pt(111) [42]. The graph at the left, shows the narrow 5σ (blue) and $2\pi^*$(red) states of CO in vacuum, the anti-bonding molecular $2\pi^*$ state is above the Fermi level. On Al(111) these states are broaden and shifted down in energy due to the interaction with the sp-states, a small contribution of the $2\pi^*$ state end up below the Fermi level. On Pt(111) in addition, the states hybridize with the d-states of the metal resulting in a bonding and anti-bonding combination with the surface, where the anti-bonding contribution of the 5σ appears above the Fermi level and the bonding contribution from the $2\pi^*$ orbital is below the Fermi level, resulting in a nett bonding interaction.

How the adsorption energies may scale with the d-band center is shown in

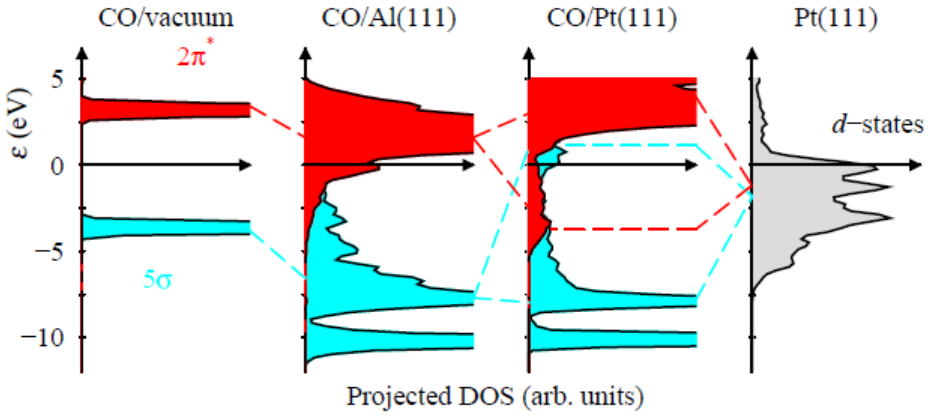

Figure 2.6: The $2\pi^*$ and 5σ band fort CO in gas phase and for Co on Al(111) and Pt(111) [42].

Figure 2.7, where the adsorption energy if CH_3 is plotted as a function of the d-band center of different surfaces on Pd. The highest adsorption energy is obtained for the corner sites, whereas the lowest energy is calculated for (111). This can be explained trough the interaction of the molecular states of CH_3 with the d-band center of the surface. When the d-band center is shifted to lower energies it comes closer to the adsorbate levels, therefore the overlap of the d-band with the molecular states of is increased stabilizing the adsorption.

2.4 The Brønstedt-Evans-Polayni relationship

The Brønstedt-Evans-Polayni relationship (BEP) [49, 50] relates the activation energies and heat of adsorption of the end product of a reaction step. DFT [51] studies have proven to be able to reproduce this linear empirical relationship, which provides a way to establish trends for catalysts design. However, the prediction relies on that the adsorbate do not change site between the studied surfaces, which is actually often the case. In Figure 2.8, the BEP relationship is shown for methane on different surfaces Pd (dots) and Pt (squares). The linear relationship shows that the more favorable the final state of the reaction is, the lower is the activation barrier. Furthermore, the figure shows that the facets of Pt, have both lower activation barriers and final state energies as compared to the corresponding facets on Pd.

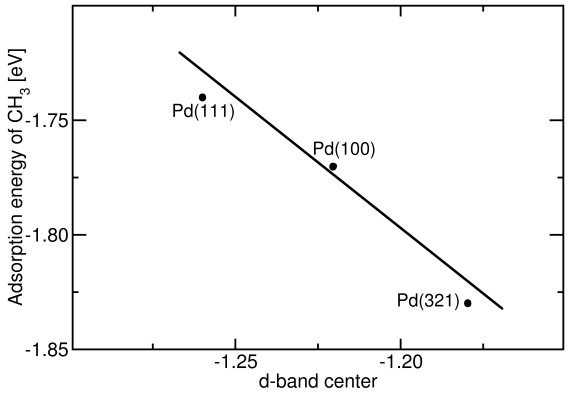

Figure 2.7: The adsorption energy of CH_3 plotted as a function of the d-band center for Pd(111), Pd(100) and Pd(321).

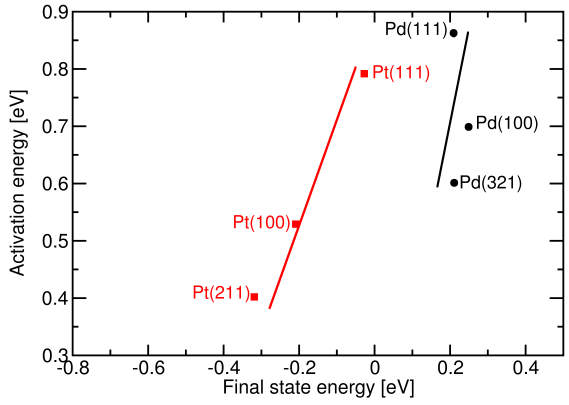

Figure 2.8: The BEP relationship for the dissociative adsorption for methane on Pd (dots) and Pt (squares).

2.5 The Sabatiers principle

As already mentioned, the strength of the adsorption of the molecules or atoms to the surface is an important property in catalytic reactions. If the molecule binds to weakly, it will not stay on the surface and will be unable to react further. On the other hand, if the adsorption energy is too strong the molecule (or atom) will poison the surface inhibiting further reactions. Paul Sabatier realized that there is an optimum of the rate of catalytic reactions as a function of adsorption

enthalpy [2]. One way to visualize this is to construct a volcano plot, where the activity of different catalyst for a certain reaction are given as a function of a parameter relating the catalysts ability to form a chemical bonds [52].

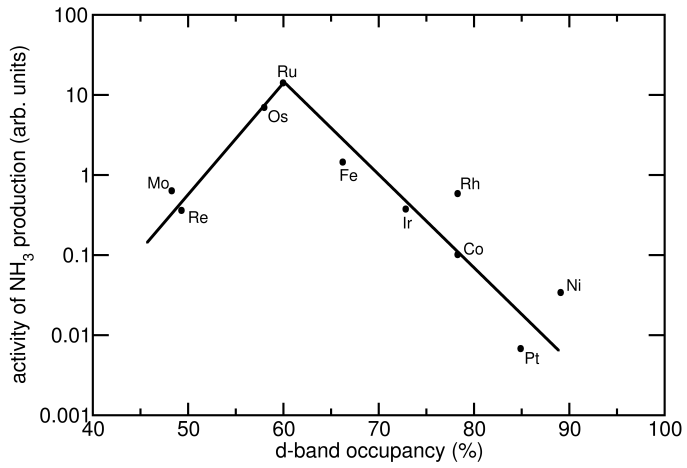

Figure 2.9: The catalytic activity of several supported transition metals as a function of the d-band occupancy. Adapted from I. Chorkendorff and J.W. Niemantsverdriet page 265 [2].

The result is an inverted triangle, where the top represent the best catalyst for the investigated reaction. Figure 2.9 shows how the activity of several metals for the synthesis of ammonia depend on the d-band occupancy. The rate determining step for this reaction is the dissociative adsorption of N_2. The metals at the left of the periodic table (Mo and Re) are capable of dissociating N_2, but the adsorption of N is too strong, whereas the metals to the right of the periodic table are unable to dissociate N_2. For this reaction, the optimum lies at 60% occupancy of the d-band [2]. The figure can be related to the d-band model, if the reaction is assumed to follow a BEP relationship in the following way: the interaction of the d-band with the adsorbate needs to generate a filling of the antibonding orbitals in the molecule in order for the molecule to dissociate. The dissociation is not a problem for the metals to the left, but the adsorption to the surface may be too strong. For the metals on the right, the antibonding states end up above the Fermi level, and N_2 is not dissociated. These kind of rationalizations of reactivity can be of great practical use when searching for suitable catalysts materials.

Chapter 3

Theory and implementation

The method chosen for the electronic structure calculations in this study is the density functional theory (DFT). DFT has during recent years become an important tool within materials and surface science. The aim of this chapter is to give a short introduction to the theory and discuss how it is implemented in the appended studies. For a more torough mathematical and theoretical review the reader is reffered to Refs. [53–55].

3.1 Density functional theory

3.1.1 The Schrödinger equation (SE)

The ability to calculate geometries, thermodynamics stabilities and reaction barriers, has a special allure to the quantum chemistry and the physics communities. The great interest is due to the information that can be extracted from such calculations. However, the task is not trivial and for many years the main approach was to find approximate solutions to the (non-relativistic) time-independent SE [56].

$$H\Psi = E\Psi \tag{3.1}$$

H is the Hamiltonian operator for a system of nuclei and electrons (an atom, a molecule or an aggregated system), Ψ is the many-body wavefunction and E is the total energy of the system. The lowest energy corresponds to the ground state energy, E_0.

To simplify the equations, it is of general practice to use atomic units, where the electron mass (m_e), the elementary charge (e), the reduced Planck's constant ($\hbar$) and the Coulomb's constant ($\frac{1}{4\pi\epsilon_0}$) are set to unity. The Hamiltonian described

in atomic units is shown in Equation 3.2.

$$H = -\sum_{i=1}^{N} \frac{1}{2}\nabla_i^2 - \sum_{A=1}^{M} \frac{1}{2M_A}\nabla_A^2 - \sum_{i=1}^{N}\sum_{A=1}^{M} \frac{Z_A}{r_{iA}} + \sum_{i=1}^{N}\sum_{j>i}^{N} \frac{1}{r_{ij}} + \sum_{A=1}^{M}\sum_{B>A}^{M} \frac{Z_A Z_B}{R_{AB}} \quad (3.2)$$

M_A is the ratio of the nucleus (A) mass and the mass of an electron. Z_A is the atomic number of the nucleus (A). ∇_i^2 and ∇_A^2 are Laplacian operators, operating with respect to the coordinates of the i:th electron and the A:th nucleus, respectively.

Each term in the Hamiltonian (Equation 3.2) represent a physical quantity: the first and second terms are the operators for the kinetic energy of the electrons and the nuclei, respectively. The third term represent the Coulomb attraction between electrons and nuclei. The two last terms represent the repulsion between electrons and between nuclei, respectively.

Nuclei are much heavier than electrons, the lightest of all, the proton, is 1800 times heavier than an electron [53]. This implies that any nucleus will move much slower than electrons, thus it is possible to consider the electrons as moving in a field of fixed nuclei. This is known as the Born-Oppenheimer approximation. Within this approximation, the kinetic energy of the nuclei, the second term in Equation 3.2, can be removed from the Hamiltonian and the last one (which is the repulsion between the nuclei) can be considered constant. The remaining terms constitute the electronic Hamiltonian (Equation 3.3) and describe the motion of N electrons in the field of M point charges.

$$H_{elec} = -\sum_{i=1}^{N} \frac{1}{2}\nabla_i^2 - \sum_{i=1}^{N}\sum_{A=1}^{M} \frac{Z_A}{r_{iA}} + \sum_{i=1}^{N}\sum_{j>i}^{N} \frac{1}{r_{ij}} = \hat{T} + \hat{V}_S + \hat{V}_{ee} \quad (3.3)$$

$\hat{T}$ is the kinetic energy of the electrons, and $\hat{V}_S$ and $\hat{V}_{ee}$ are the Coulomb interaction of the nuclei and electrons and of the electrons, respectively. The solution of the SE with H_{elec} depends on the electronic coordinates, while the nuclear coordinates are only treated as parameters. The total energy is the sum of E_{elec} and the nuclear repulsion term which is the last term in Equation 3.2. The attraction between nuclei and electrons $\hat{V}_s$ is often termed external potential because it can include other external fields (magnetic and/or electric). The total ground-state energy (E_0) can be expressed as a function of the coordinates of the nuclei $E(\vec{R}_i)$ which gives the potential energy surface (PES).

However, the equation has been solved exactly only for one electron systems,

such as the hydrogen atom or H_2^+. There have been two main strategies to solve this problem approximatively: one based on solving the electronic many-body wavefunction, the first successful version and the predecessor of methods is the Hartree-Fock scheme [57–61]. However, wavefunction-based methods are computationally very expensive. In particular, if high accuracy is required. The second methodology is based on approaching SE in an alternative way, using the electron density instead of the many-body wavefunction $\rho(\vec{r})$ as the basic variable.

3.1.2 The Hohenberg-Kohn theorems

Identifying the electron density as the key quantity simplifies the problem, because it depends only on three coordinates as compared to 3N (where N is the number of electrons) for the wavefunction approach. One early attempt along this line was the Thomas Fermi model, however, the real breakthrough for density functional theories was a paper by Hohenberg and Kohn from 1964.

The paper proposed two theorems. The first theorem showed in a very simple way that the total energy of a system is a unique functional of the electron density. The total energy expression can be divided into two parts, one part that is system dependent and another part that is universal and not depending on N, R_A and Z_A:

$$E[\rho] = \int \underbrace{\rho(\vec{r})V_S d\vec{r}}_{\text{system dependent}} + \underbrace{T[\rho] + E_{ee}[\rho]}_{\text{universally valid}}. \tag{3.4}$$

The system independent part is called the *Hohenberg-Kohn* functional:

$$E[\rho] = \int \rho(\vec{r})V_S d\vec{r} + F_{HK}[\rho] \tag{3.5}$$

If the Hohenberg-Kohn functional is provided with an arbitrary density it gives the expectation value $\langle\Psi|\hat{T} + \hat{V}_{ee}|\Psi\rangle$. This includes the sum of the kinetic energy and the electron-electron repulsion operator with the ground state wavefunction Ψ connected to this density. If the *Hohenberg-Kohn* functional was known exactly, the electronic problem could be solved exactly.

The second theorem states that the ground state density can be obtained trough a minimization and by knowing the ground state density $\rho(\vec{r})$ it is possible to obtain the ground state energy E_0. One way to approach this problem is according to the variational principle, by means of a constrained search approach. Furthermore, there cannot be two different external potentials V_S yielding the same ground state density, and the density uniquely specifies the external

potential.

The task is separated into three steps: The first steps is a search over the subset of all the antisymmetric many body-wave function, denoted Ψ^X, that upon quadrature generates a particular density ρ_X. The density is under the constraint that it must integrate to the correct number of electrons. This search gives the wave function Ψ^X_{min} that gives the lowest energy for the given density ρ_X. In the second step the search involves all densities. The final step is to identify the density among the many that is the ground state density. This is represented in Equation 3.6, the inner minimization corresponds to the first step and the outer minimization corresponds to the second step.

$$E_0 = \min_{\rho \to N} \left(\min_{\Psi \to \rho} \left\langle \Psi^X | \hat{T} + \hat{V}_{ext} + \hat{V}_{ee} | \Psi^X \right\rangle \right) \tag{3.6}$$

3.1.3 Kohn-Sham equations

One year after the publication of the Hohenberg-Kohn theorems, a paper by Kohn and Sham [62] suggested a way to approach the unknown universal functional. The idea behind this was that the main problem with density functionals are connected with the way the kinetic energy is determined. The paper introduced the idea of a non-interacting reference system built from a set of one-electron states (φ_i) which are connected to the density according to:

$$\rho = \sum_i |\varphi_i|^2 \tag{3.7}$$

Consequently, the dominant part of the kinetic energy can be computed with good accuracy. The remaining part is mixed with the non-classical electron-electron repulsion (also unknown but small). The major part of the energy is then computed exactly and just a small part is determined by an approximate functional. Recalling that the universal functional can be divided into two contributions: Kinetic energy and the electron interaction V_{ee}, the latter is further divided into two contributions, classical ($J[\rho]$) and non classical ($E_{ncl}[\rho(\vec{r})]$) electron interaction.

$$F[\rho(\vec{r})] = T_S[\rho(\vec{r})] + J[\rho(\vec{r})] + E_{ncl}[\rho(\vec{r})] \tag{3.8}$$

E_{ncl} contains the self-interaction correction, that is introduced to correct for the unphysical self interaction that arises in $J[\rho(\vec{r})]$. It also contains electron exchange and correlation. The kinetic energy of the non-interacting reference system (which

has the same density as the real one) is computed according to:

$$T_S = -\frac{1}{2}\sum_i^N \left\langle \varphi_i \middle| \nabla^2 \middle| \varphi_i \right\rangle \tag{3.9}$$

The difference between the real kinetic energy and the non interacting one is accounted for with the introduction of a separate functional:

$$F[\rho(\vec{r})] = T_S[\rho(\vec{r})] + J[\rho(\vec{r})] + E_{XC}[\rho(\vec{r})] \tag{3.10}$$

were E_{XC} is the *exchange correlation energy* defined as:

$$E_{XC}[\rho] \equiv \big(T[\rho] - T_S[\rho]\big) + \big(E_{ee}[\rho] - J[\rho]\big) = T_C[\rho] + E_{ncl}[\rho] \tag{3.11}$$

The residual part of the true kinetic energy $T_C[\rho]$ is simply added to the non-classical electrostatic contributions. The functional contains all that is unknown.

3.1.4 Exchange and correlation functionals

The Kohn-Sham formalism allows for an exact treatment of most of the contributions to the electronic energy, including the major fraction of the kinetic energy, the remaining unknown contributions are folded into the exchange-correlation functional E_{XC}. The quality of the density functional approach depends on the accuracy of the approximation to E_{XC}.

The exact formalism for the exchange-correlation potential is not known. The contribution of E_{XC} to the total energy is small (for the total valence energy of the Mg atom it corresponds roughly to $\sim 6\%$ [63]). However, the accuracy of the method depends on this contribution. If we would know the exact form, we would be able to calculate the exact energy of the system. Hence, numerous approximation have been proposed.

In an article by P. Perdew and K. Schmidt [64] a ladder of approximations to the exchange correlation functionals is described. Where the lowest rungs are levels where only the density is used. The next level corresponds to the addition of gradients. Higher levels are typically (but not always) more computationally demanding. The first rung corresponds to the Local Density Approximation (LDA).

Local Density Approximation

The Local Density Approximation [62] is based the idea of a uniform electron gas. In this system, the electrons move in the background of a positive charge distribution such that the ensemble is neutral. This picture resembles the model of an idealized metal consisting of a perfect crystal of valence electrons and positive jellium background. The uniform electron gas is an important concept in DFT as it is the only system for which the form of the exchange and correlation functionals are known. The E_{XC} within the LDA formalism can be written as:

$$E_{XC}^{LDA} = \int \rho(\vec{r})\varepsilon_{XC}(\rho(\vec{r}))d\vec{r} \tag{3.12}$$

where ε_{XC} is the exchange-correlation energy density for a uniform electron gas $\rho(\vec{r})$. ε_{XC} can be divided into exchange and correlation contributions.

$$\varepsilon_{XC}(\rho(\vec{r})) = \varepsilon_X(\rho(\vec{r})) + \varepsilon_C(\rho(\vec{r})). \tag{3.13}$$

The term ε_X represents the exchange energy of a uniform electron gas and is equal to the one derived by Slater in the Hartree Fock exchange [65].

$$\varepsilon_X = -\frac{3}{4}\sqrt[3]{\frac{3\rho(\vec{r})}{\pi}} \tag{3.14}$$

No explicit expression is known for the correlation part. However, exact numerical quantum Monte Carlo simulations of the homogeneous gas by Ceperly and Alder [66] hase been used to obtain analytical expressions. One of the most known was proposed by Vosko, Wilk, and Nusair (VWN) [67]. LDA yields reasonable geometries and vibrational frequencies [63] but overestimates atomization energies [64].

Generalized Gradient Approximation

The next step after LDA is to use not only the information about the density (ρ) at a particular coordinate $\vec{r}$, but to also supplement this with information about the gradient of the charge density (∇) to account for the non-homogeneity of the density.

$$E_{XC}^{GGA}[\rho] = \int f(\rho, \nabla\rho)d\vec{r} \tag{3.15}$$

The exchange part of E_{XC}^{GGA} is rewritten as:

$$E_X^{GGA} = E_X^{LDA} - \sum_\sigma \int F(s_\sigma)\rho_\sigma^{4/3}(\vec{r})d\vec{r}, \tag{3.16}$$

Where s_σ is defined as the reduced gradient for spin σ according to:

$$s_\sigma(\vec{r}) = \frac{|\nabla\rho_\sigma(\vec{r})|}{\rho_\sigma^{4/3}(\vec{r})} \tag{3.17}$$

The GGA functionals yield lattice parameters and bulk moduli that are close to experimental values for the first row of transition metals. Cohesive energies are over-corrected as compared to LDA yielding values that are too low [68]. There are several GGA functionals, the one used in this thesis is the one proposed by Perdew, Burke and Ernzerhof (PBE) [69].

3.2 DFT implementation

Although the theory mentioned above, provides a theoretical base explicit calculations require numerical approximations to describe orbitals and densities and to evaluate potential and energies. These introduce further approximations that are numerical in nature to be able to perform calculations. [70]. One problem is the representation of the electronic orbitals. The core states are more localized than the valence states. For the valence states to be orthogonal to the core, they must oscillate rapidly, which makes them harder to represent. This leads to the introduction of the frozen core approximation, where the core states are assumed to remain constant during the chemical reaction. The projector augmented waves (PAW) description is based on this assumption.

3.2.1 Projector augmented waves

Due to the rapid oscillations near the cores of the wavefunctions, they require a fine grid to be represented accurately. At longer distances the functions are smother and easier to represent. A way to approach the problem is to describe the core regions as an effective potential. The PAW method proposes to use projectors acting on smooth valence wavefunctions, $\tilde{\psi}$ which are the primary objects in the calculations, introducing auxiliary localized functions, that keep all the information of the core states. It is important to note, that the information

of the core electrons is available, giving access to the full electron density. The smooth part of a valence wavefunction is denoted $\tilde{\psi}$, the linear transformation $\psi = T\tilde{\psi}$ relates the set of all electron valence functions $\psi_n(\vec{r})$ to the smooth functions $\tilde{\psi}_n(\vec{r})$. The transformation is assumed to be unity except for a sphere defined near the nucleus, $T = 1 + \sum_A \hat{T}^A$, where $\hat{T}^A$ is the atom centered transformation. This leads to the following expansion of the true wavefunction [70],

$$|\psi_n\rangle = |\tilde{\psi}_n\rangle + \sum_A (|\psi_n^A\rangle - |\tilde{\psi_n^A}\rangle) = |\tilde{\psi}_n\rangle \sum_{i,A} (|\phi_i^A\rangle - |\tilde{\phi_i^A}\rangle)\langle\tilde{p}_i^A|\tilde{\psi}_n\rangle, \tag{3.18}$$

were the sums are over atomic corrections inside the augmentation sphere for each atom. These are formulated in terms of partial waves $(\phi_i^A, \tilde{\phi}_i^A)$, with the different oscillatory behavior, and local projectors (p_i^a). Hence, the true Kohn-Sham wavefunction is divided into two parts; one for valence electrons outside the atomic cores and the other for all the contributions near the atom. The latter can be pre-calculated and stored for each chemical element and the main computational effort of the calculation is focused on the valence electrons.

3.2.2 PAW in real space grids

The PAW method is implemented in GPAW using reals-space multigrid discretization. Where different grids are used in the two different regions (inside and outside the augmentation sphere). The physical quantities are represented numerically by their value in the grid point. The integrals are approximated by summation over the grid-points, and the differentiation is performed according to the finite difference approximation. The use of real space grid has several advantages, where the most important one is that the parallelization of the calculation is easier in the real space. Making it possible to use massively parallelized computer clusters enabling calculations over more complex and larger systems [71].

To asses which grid-spacing was needed to have sufficient accuracy at the lowest computational cost of our system, a test was performed and is shown in Table 3.1. The chosen grid spacing throughout this thesis is 0.18 Å. The results show no real correlation between increasing the grid (basis set) and increase in accuracy. The reason behind this is that already at a grid spacing of 0.22 Å the system is converged, and the difference is between the different values at each grid spacing are due to numerical noise.

Table 3.1: Adsorption energies (eV) of CH_3 and H with different grid spacings on Pd(100).

Adsorbate	Grid spacing[Å]						
	0.22	0.20	0.18	0.17	0.16	0.15	0.14
CH_3	-1.73	-1.78	-1.78	-1.77	-1.81	-1.75	-1.77
H	-2.7	-2.73	-2.71	-2.71	-2.75	-2.71	-2.71

Chapter 4

Modeling surface reactions

In order to correctly represent the studied systems, it is important to know how to build models that as accurately as possible reproduce the most important features. This includes, e.g. how surfaces are modeled and how the calculated reaction landscapes are implemented in microkinetic models.

4.1 DFT modeling

To approximate the surfaces, using periodic boundaries, a slab model has been used. This model uses the periodicity of the bulk and repeats the chosen cell infinitely in all directions. However, for a surface, the periodicity is only desired in two directions (x and y), whereas the periodicity in the z axis can be a problem. This is solved by separating the cells with a vacuum in the z-direction.

It is important to choose enough vacuum to ensure that the cells do not interact with each other in the z-direction. A figure of a 4 layer slab for Pd(100) with a vacuum of 12 Å is shown in Figure 4.1. Figure 4.1a) shows a side view of the computational cell, b) shows the periodicity in the z-direction, and c) illustrates the periodicity in the x and y directions. Sometimes for the purpose of modeling a surface, only periodicity in the x-direction is needed.

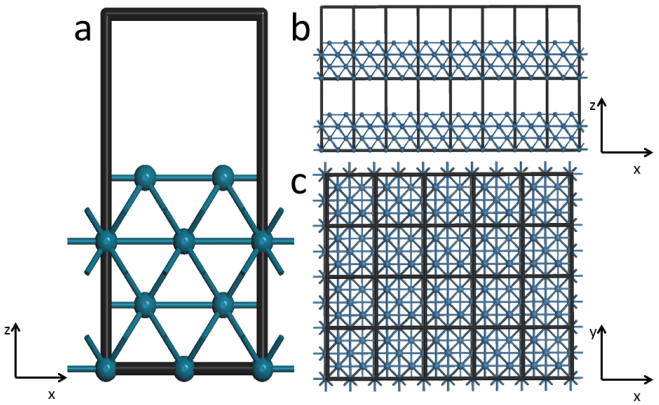

Figure 4.1: Model of a (100) surface. a) The computational cell b) The computational cell is repeated in the z- and x-directions. A proper vacuum between two cells is needed in the z-direction to ensure that the two layers do not interact. c) The periodicity in the x and y directions.

The computational cost increases with the number of atoms, hence, there is a trade off between computational cost and the best description of the system. Figure 4.2 shows a convergence test for Pd(100) where the adsorption energy of the methyl group is plotted against the number of layers of the slab, for two cases: i) when the two bottom layers are constrained to the bulk positions (black) and ii) for the unconstrained system (dotted). The figure shows that at 2 layers, the adsorption energy is well converged and that after 3 layers, the adsorption energy is not affected by the constrained bottom layers. The number of layers of the slabs in the appended papers are 4 with the two bottom layers constrained.

The periodic boundary conditions have another consequence when modeling adsorbates on the surface. The adsorbate coverages is determined by the chosen cell size. This is shown in Figure 4.3 where a) is representing the computational cell alone, and b) shows the coverage of the surface, using a p(2x2) computational cell. The coverage is in this case 0.25 ML. The particular example shown here is CO adsorbed onto a bridge position on Pd(100). The coverage of the surface is an important factor as lateral interactions directly affects the value of the adsorption energy. This is discussed further in Section 4.4.1.

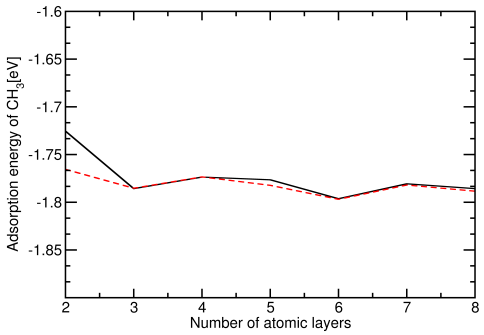

Figure 4.2: Convergence test performed on Pd(100) where the adsorption energy of the methyl group is evaluated as a function of the number of layers in the slab. The solid line represents the slab with the two bottom layers constrained and the dashed line shows the results for the unconstrained case.

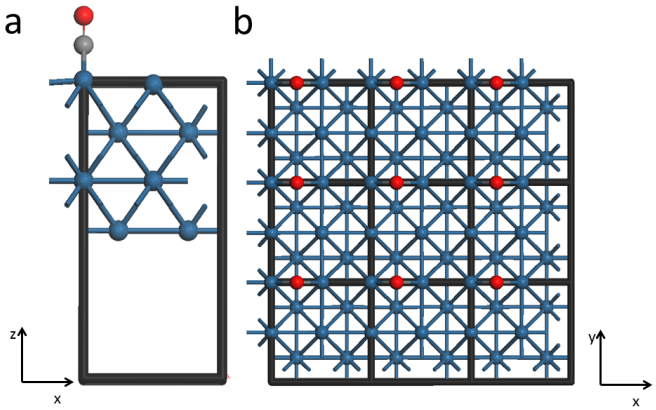

Figure 4.3: a) Side view of CO adsorbed on Pd(100) b) Top view of Co adsorbed on Pd(100). The coverage is 0.25 ML.

4.2 Microkinetic modeling

A microkinetic model translates the reaction energy landscapes, including activation barriers into reaction rates. There are two models included in the present study, the first (Paper I) is a mix between both statistical mechanics and experimental values. The second model (Paper II) uses only statistical mechanics as

a link between the adsorption energies, activation barriers and vibrational spectrum from DFT and the kinetics of the entire reaction. Both models are based on two main approximations, i) the mean field approximation, and ii) the steady state approximation. In addition a rate determining step that controls the overall rate of the reaction was assumed in Paper II.

The mean field approximation [2] assumes that all adsorbed species are randomly distributed over the surface. This is a good approximation if the surface is uniform. Lateral interactions between adsorbates are treated in a mean field fashion, i.e. depending only on the coverage and not on the local configuration. This assumption works well for systems where the interaction of adsorbates is repulsive (as the case for oxygen atoms), but less well for attractive interactions where adsorbates forms small islands and the reactions might occur on the boundaries of these islands. The steady state approximation is based on the assumption there is no time dependence in the coverage ($\frac{d\theta^*}{dt} = 0$). This is not the case when the system is starting up where the system normally shows a transient behavior.

The assumption that there is one step in thre reaction landscape that controls the rate of the reaction leads to the quasi-equilibrium approximation, which is based on the assumption that all the other reaction steps are in equilibrium. There is the possibility that the system changes rate determining step (RDS) if the reaction conditions are changed. However, this complication is beyond the scope of this study.

A short description of the microkinetic model for carbon monoxide oxidation in Paper I is presented here. The model is based on an already developed kinetic models for the reaction [72, 73]. The assumed reaction path for CO oxidation is a Langmuir-Hinshelwood scheme:

$$
\begin{aligned}
CO + * &\rightleftharpoons CO* \\
O_2 + 2* &\rightarrow 2O* \\
CO* + O* &\rightarrow CO_2 + *
\end{aligned}
$$

Here, * denotes empty surface sites. The rate equations for the steady state case is:

$$
\begin{aligned}
s^0_{CO}(1-\theta^2_{CO})k^+_1 p_{CO} - k^-_1\theta_{CO} - k^+_3\theta_{CO}\theta_O = 0 \\
2s^0_O(1-\theta_{CO}-\theta_O)^2 k^+_2 p_{O_2} - k^-_2 k^+_3 \theta_{CO}\theta_O = 0
\end{aligned}
\tag{4.1}
$$

Here, s^0_{CO} and s^0_O are the sticking coefficients for CO and O, respectively, θ_{CO} and θ_{CO} represent the surface coverages, and p_{CO} and p_O are the partial pressures. The rate constants are defined as follows:

$$\begin{aligned} k_1^- &= \nu^d_{CO} e^{-E^d_{CO}(1-\alpha\theta_{CO})/k_B T} \\ k_3^+ &= \nu^r e^{-E^r(1-\beta\theta_{CO})/k_B T} \\ k_1^+; k_2^+ &= \frac{1}{N_0\sqrt{2\pi M k_B T}} \end{aligned} \tag{4.2}$$

T is the temperature, k_B is the Boltzmann constant, M is the mass of the considered molecule and N_0 is the number of sites per area. A linear coverage dependence is assumed for both adsorption energies and barriers, α and β are set close to 0.5. The pre-exponential factors and sticking coefficients are set according to experimental estimates [72, 73], namely $k_1^- = 10^{15} s^{-1}$, $k_1^- = 10^{14} s^{-1}$, $s^0_{CO} = 0.84$ and $s^0_O = 0.02$.

A short description of how the different reaction steps for methane oxidation are the described in the microkinetic model in Paper II is presented below. As an example the two first steps in methane dissociation are discussed:

$$CH_4 + * \rightleftharpoons CH_4^* \ \ (fast) \tag{4.3}$$

$$CH_4^* \rightarrow CH_3^* + H \ \ (slow) \tag{4.4}$$

the rate equation of Reactions 4.3 (within the quasi equilibrium assumption) becomes:

$$r_{fast} = p_{CH_4} k_1^+ \theta_* - k_1^- \theta_{CH_4} \approx 0 \tag{4.5}$$

Here, p_{CH_4} is the pressure of CH_4, k_1^+, k_1^- are the rate constants for the forward and backward reactions, respectively. θ_* and θ_{CH_4} denote the empty sites and the coverage of CH_4. The coverage of methane (θ_{CH_4}) can be expressed as:

$$\theta_{CH_4} = p_{CH_4} K_1 \theta_*; \ K_1 = \frac{k_1^+}{k_1^-} \tag{4.6}$$

K_1 is the equilibrium constant which can be expressed as the partition functions of the product and the reactant and their difference in energy:

$$K_1 = \frac{z_{CH_4^*}}{z_{CH_4}} e^{\Delta E/k_B T} \tag{4.7}$$

The partition function is defined as:

$$z_i = z_{i,trans} z_{i,rot} z_{i,vib} \tag{4.8}$$

The vibrations are calculated using a vibrational analysis within the harmonic oscillator approximation. The rotational constants are taken from literature for gas-phase molecules [74] or calculated as frustrated rotations (low frequency vibrations) for adsorbates.

Reaction 4.4 is assumed to be the slow reaction, i.e. the rate determining step (RDS). Here only the forward reaction is considered:

$$r_{slow} = k_2^+ \theta_{CH_4} \theta_* = k_2^+ p_{CH_4} K_1 \theta_*^2 \tag{4.9}$$

The forward reaction constant can be written as:

$$k_2^+ = \frac{k_B T}{h} \frac{z_{CH_4^\ddagger}}{z_{CH_4^*}} e^{\Delta E / k_B T} \tag{4.10}$$

Where the energy difference is the calculated activation barrier. The rate of the reaction becomes:

$$r_{slow} = p_{CH_4} K_1 \frac{k_B T}{h} \frac{z_{CH_4^\ddagger}}{z_{CH_4^*}} e^{\Delta E / k_B T} \tag{4.11}$$

Substituting K_1 gives:

$$r_{slow} = p_{CH_4} \frac{k_B T}{h} \frac{z_{CH_4^\ddagger}}{z_{CH_4^*}} \frac{z_{CH_4^*}}{z_{CH_4}} e^{\Delta E / k_B T} \tag{4.12}$$

This makes the rate independent of $z_{CH_4^*}$ as long as the coverage of CH_4 is sufficiently low. The total reaction path for methane used in the model is as follows:

$$\begin{aligned}
* + CH_4(g) &\rightleftharpoons CH_4^* \\
* + CH_4^* &\rightleftharpoons CH_3^* + H^* \\
* + CH_3^* &\rightleftharpoons CH_2^* + H^* \\
* + CH_2^* &\rightleftharpoons CH^* + H^* \\
* + CH^* &\rightleftharpoons C^* + H^*
\end{aligned}$$

Here, (g) and * denote gas phase and adsorbed molecules, respectively. The oxidation of the intermediates, adsorbed carbon and adsorbed hydrogen, into

products is modeled according to:

$$
\begin{aligned}
2* + O_2(g) &\rightleftharpoons 2O^* \\
C^* + O^* &\rightleftharpoons CO^* + * \\
CO^* + O^* &\rightleftharpoons CO_2(g) + 2* \\
H^* + O^* &\rightleftharpoons OH^* + * \\
OH^* + H^* &\rightleftharpoons H_2O^* + * \qquad (4.13) \\
OH^* + OH^* &\rightleftharpoons H_2O^* + O^* \qquad (4.14) \\
H_2O^* &\rightleftharpoons H_2O(g) + *
\end{aligned}
$$

There are two possible paths for water formation i) hydroxyl reacts with one hydrogen atom (Equation 4.13) or ii) recombination of two hydroxyls (Equation 4.14).

4.3 Transition state and the potential energy surface

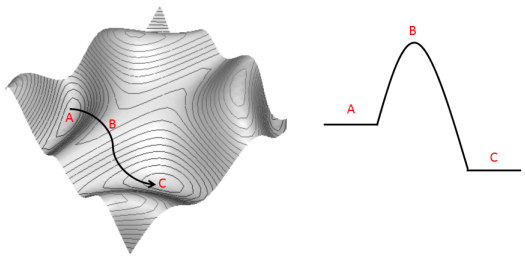

Figure 4.4: Schematic representation of a PES. A and C are minima, to get from A to C, there is a intermediate high energy state (B).

The potential energy surface (PES) is an important property because it determines the energy required to go from one minimum to another. Which is relevant when discussing activation barriers and transition states. A schematic picture of a PES is shown in Figure 4.4.

A chemical reaction often requires a certain temperature, even if the reaction is exothermic, this is because for the reactants to convert into the product, there is a need to cross intermediate structures with higher energy than both reactant (A)

and the product (C). The intermediate complex is often called activated complex or transition state (B). The transition state complex is a saddle point in the PES, thus a minimum in all coordinates except the reaction coordinate. It represents the energetic barrier that the reactants surpass to become the products.

In both appended papers, the activation barriers are calculated using constrained optimizations. In this method, several images between products and reactants are calculated, constraining a bond in the reaction coordinate of interest, but allowing the rest of the system to relax. The constrained bond is either elongated or shortened between images. The images are interpolated yielding a reaction path. Other methods are available for this type of calculations, are the nudged elastic band method (NEB) [75] or the conjugate gradient methods [76]. Also a vibrational analysis of the activation complex is often performed to ensure that the geometry corresponds to a real transition state, which can be corroborated if one of the vibrations is imaginary.

4.4 Reaction Rate

Transition states often determine the kinetics of a reaction; the higher the barrier to climb, the higher the temperature (energy) needed for the reaction to occur. However, there are other parameters that affect the rate of a reaction, one is the preexponential factor. The rate of the transition state (r_{tst}) can be expressed as:

$$r_{tst} = \frac{k_B T}{h} e^{-\Delta G_0^{\ddagger}/k_B T} = \frac{k_B T}{h} e^{\Delta S_0^{\ddagger}/k_B T} e^{\Delta H_0^{\ddagger}/k_B T} \tag{4.15}$$

k_B is Boltzmann's constant and h denotes Planck's constant. $\Delta G_0^{\ddagger}$ represents the difference in Gibbs free energy and $\Delta S_0^{\ddagger}$ and $\Delta H_0^{\ddagger}$ represent the entropy and enthalpy differences, respectively. The enthalpy is calculated from first principles and corresponds to the activation barrier. The pre-exponential factor is defined as:

$$\nu_{tst} \equiv \frac{k_B T}{h} e^{\Delta S_0^{\ddagger}/k_B T} \tag{4.16}$$

The pre-exponential factor is calculated from the partition functions, which in turn are evaluated trough vibrational analysis. If going to the transition state results in a gain in entropy, the pre-exponential becomes larger and increases the rate of the reaction. This is often referred to as a loose transition state [2]. If instead the entropy in the transition state is lower in entropy as compared to the reactants, then the transitions state is called a tight transition state [2]. This

is typical for dissociations over surfaces, and one example of this is dissociative adsorption of methane. Typical values for pre-exponential factors that for loose transition states are values above 10^{13} [2]. Tight pre-exponential factors have values below 10^{13}. In our calculations the value for methanes dissociative adsorption is 6×10^{11} thereby classifying as a tight transition state. For the formation of water through the OH+H reaction, the pre-exponential factor is 1.14×10^{13} which indicates that the vibrations rotations and translations in the reactants are neither more or less restricted when going to the transition state complex. Both pre-exponential factors are calculated for Pd(111) at 300 K.

4.4.1 Coverage effects

As already mentioned, the coverage of adsorbates can have a substantial impact on the thermodynamics of the reaction landscape. Figure 4.5 shows the adsorption of oxygen as a function of coverage for Pd(111) and Pd(100).

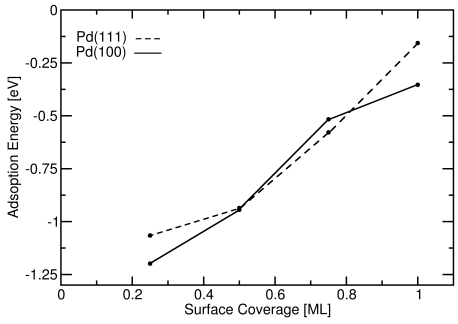

Figure 4.5: The oxygen adsorption energy as a function of coverage for Pd(111) and Pd(100).

The higher the coverage, the less stable is the adsorption of oxygen. The case with oxygen is probably one of the more extreme cases, where the adsorption energy with respect to O_2 in the gas phase changes drastically, from -1.1 eV to -0.15 eV for the Pd(111) surface.

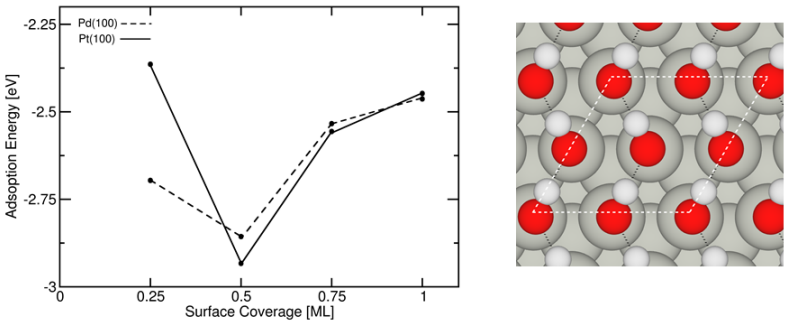

Figure 4.6: Left: The reported surface coverage of Pd(111) and Pt(111) as a function of the adsorption energy of hydroxyl-groups. Right: the prefered adsoption site on Pt(111) of hydroxyl groups at a coverage of 1 ML.

Attractive interactions as formation of hydrogen bonds have the opposite effect as compared to the above mentioned oxygen example, and can stabilize the adsorption energy of hydroxyl groups at higher coverages. The adsorption energy of OH groups is shown in Figure 4.6 as a function of the coverage. Here, the relationship is not linear, and the stabilization depends on both the lateral repulsion of the oxygen atoms in the hydroxyl-groups and on the formation of hydrogen bonds. The stabilizing effect can change the preferred adsorption site, when the coverage is increased. In Figure 4.6 at the right it is shown that OH groups at a coverage of 1 ML prefer the top site, however, at a coverage of 0.25 the preferred adsorption site is fcc hollow. On the top site the molecules are able to coordinate to each other forming hydrogen bonds. There is a gain in energy as the formation of the bonds is stronger then the loss when going form a fcc hollow to an atop site.

Chapter 5

Oxidation of carbon monoxide

Carbon monoxide oxidation is a well studied reaction, both experimentally [7,77–79] and theoretically [28–30, 32, 80, 81]. This chapter gives a short introduction to the subject, discussing the most important results and conclusions originating from Paper I.

5.1 Introduction to CO oxidation

Between 50 and 90 % of the total amount of emitted hydrocarbons from a car with a three-way catalyst, are released during the cold start [5, 23]. Cold start refers to the period when the engine is running but the catalyst is still cold. At these conditions, CO poisons the catalyst affecting the overall performance of the catalyst. There are three approaches to solve the cold start problem [82] i) change the gas composition during the start up period ii) heat the catalyst through advanced methods so it quickly reaches the critical temperature and iii) lower the critical temperature by design of catalysts for low temperature oxidation. The latter alternative seems to be the most energy efficient.

On Pt(111), CO is measured to adsorb associatively when the temperature reaches 160 K and to desorb at 400 K [83] and O_2 is shown to be adsorbed associatively at 77 K but dissociatively already at 104 K [41]. However, at low temperatures the surface is poisoned by CO. There are mainly three reasons behind the self-poisoning of CO i) the probability of CO sticking to the surface is much higher than for oxygen: the sticking probability of CO is 0.8 at zero coverage decreasing with increasing coverage to ∼0.3 at 0.5 ML, whereas for oxygen the sticking probability is 0.064 at zero coverage, also decreasing with coverage [84]. ii) CO adsorbs associatively and O_2 dissociatively i.e. CO needs one surface site

while O_2 needs two. iii) CO may block the adsorption of O_2 [85], due to lateral interactions between the two adsorbates. These are the reasons why CO oxidation on Pt(111) (and on several other surfaces) is known to have bi-stable kinetics. This implies that there are two modes in which CO can oxidize, depending on the history of the catalyst. The first one is a slow rate mode where CO is self-poisoned and the second one in oxygen excess, where the rate is much higher. The bi-stability of carbon monoxide oxidation has other consequences, as kinetic phase transitions and oscillatory kinetics with the formation of standing waves. These phenomena have been extensively studied in the literature [7,24,31,78,79,85,86].

5.2 Studying the bi-stability on Pd and Pt

Paper I is a collaboration between an experimental group at Vienna University of Technology and the computational catalysis group here at Chalmers. The experimental sample consisted of a polycrystalline foils of Pd and Pt, which allowed all surfaces, namely (111), (100) and (110) to be exposed to the same environment. The foil was monitored with photoemission electron microscopy (PEEM), providing laterally resolved kinetic information from the different surfaces and a mass spectrometer that gave the average CO_2 formation. The experiment were performed at very low pressures (p_{CO}=5.8 $\times 10^{-6}$ and p_O=1.3 $\times 10^{-5}$, i.e in the oxygen excess). Both temperature and pressured were ramped (372-493 K and varying the partial pressure of CO up to 2.5×10^{-5}). Noticeable is that the kinetic transition points, when going from the low activity region to the high activity region, are in quantitative agreement for the isothermal experiments and the isobaric ones. Thereby allowing a link between the typical surface science (isothermal) with the typical catalysis approaches (isobaric).

The experimental kinetic phase diagrams were compared to the ones calculated from first principles. Figure 5.1a) shows the simulated kinetic phase diagrams for Pd(111) and Pt(111) and b) the simulated local kinetic phase diagrams of Pt(110), Pt(100) and Pt(111). The main conclusion from Paper I is that the reaction is highly structure sensitive for both metals, with each surface having different ignition and extinction temperatures. The general differences between the two metals were that for Pd, the transition from the low activity regime to the one with high activity occurs at higher CO partial pressures with a narrower bi-stability range as compared with Pt. Thus the conclusion is that more CO is needed to poison Pd, and a lower oxygen to CO ratio is sufficient to reactivate the

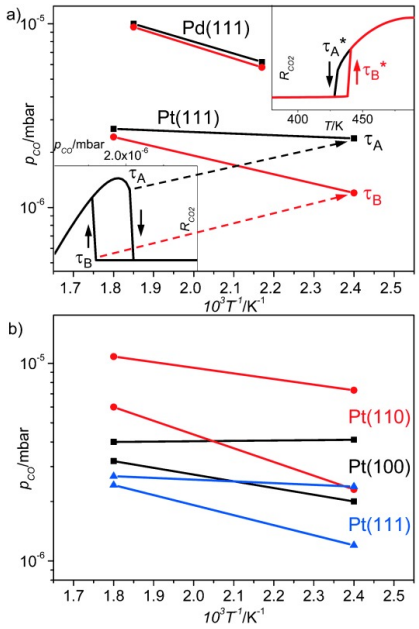

Figure 5.1: a) Simulated kinetic phase diagrams for Pd(111) and Pt(111) at $p_{o2} = 1.3 \times 10^{-5}$mbar. The left inset shows the hysteresis curve for Pt(111) at 417 K and the right inset shows the ignition/extinction curve for Pd(111) at $p_{co} = 5.8 \times 10^{-6}$mbar. b) Simulated local kinetic phase diagrams of Pt(110), Pt(100) and Pt(111) at $p_{o_2} = 1.3 \times 10^{-5}$mbar.

surface. These results were tested with the DFT data and a microkinetic model that were in good agreement with the measurements. Showing that the reason for the higher tolerance to CO poisoning of Pd as compared to Pt is due to the higher oxygen adsorption energy. This explains that higher CO partial pressures are needed to poison the surfaces. Moreover, the sticking coefficient (taken from experiments) of oxygen is higher on Pd explaining why Pd reactivates at higher CO partial pressures. For this reaction, the typical surface science approach and the microkinetic model yield the same results as common technical approaches, if the latter are done at low pressures. Furthermore, an important conclusion is that the microkinetic model successfully reproduces the experimental results in a close to quantitative manner.

Chapter 6

Methane oxidation

Methane oxidation over Pd and Pt is studied in Paper II. This chapter introduces the subject and gives a short account of the most important results and conclusions of Paper II.

6.1 Introduction to methane oxidation

Natural gas, is a viable bridge between fossil and renewable energy sources. One advantage with the natural gas vehicle (NGV) is the low engine out emissions of NO_x and SO_x, which are below current emissions standards [21]. Methane, which is the main component of natural gas, is fairly inert due to the high symmetry of the molecule and due to the strength of the carbon-hydrogen bond. Generally for alkanes, the shorter the length of the chain, the higher is the activation barrier for oxidation. Thus, methane is the least reactive alkane [87]. However, methane has the highest hydrogen to carbon ratio producing the most amount of energy per formed mole of CO_2 [88], making it the greenest fossil fuel. Nevertheless, as methane is a potent greenhouse gas (with 20 times the CO global warming potential per kg [22]) aftertreatment systems have to be used to ensure complete oxidation of CH_4.

The mechanismes involved in the complete oxidation of methane for aftertreatment purposes, is a long standing puzzle and has been the subject of extensive studies [89], from surface science experiments to reactor [21, 90–96] and kinetic studies [97, 98]. The complexity of the subject lies in the lack of agreement between different experiments with each other and with theory, together with the inherent difficulty in heterogeneous catalysis of relating the results of different time and length scales.

As mentioned in the Introduction, the active sites in a catalyst are the surfaces of small metal nano-particles deposited on a metaloxide support. The particles interact with the support which influences their shape. The strength of interaction depends on which support is used [40]. Furthermore, the support can sometimes act as an active site and oxygen storage site [90,93]. In addition, the shape of the particle is not static, instead the particles change in response to the environment [6]. The interaction of the metal particle with its support and how this affects the reactivity and activity of the catalyst is not studied in this report.

The second complication is more fundamental, namely how to understand the active phase of Pd. At lean conditions (in oxygen excess) most authors agree on that the stable phase is PdO, although the temperature range depends on support and reaction conditions [92,97,99–104]. However, whether the stable phase is also the active phase, has been a question of debate. Whereas measurements indicated that the activity of Pd was strongly correlated to oxide phases [92, 101, 104], DFT studies showed that the activation barrier for the dissociative adsorption of methane on Pd oxides was higher than on the metal [105, 106].

Hellman et al. [10] showed that there is a single active site on PdO which adsorbs methane differently. Methane has in general a very low adsorption energy on the metal facets. Depending on facet on Pd, it ranges from 0 to -0.07 eV, calculated with PBE, which imply a weak physisorption. The molecule coordinates one hydrogen towards a metal atom generating a slight image charge in the metal. The dissociation proceeds over a top site, where only one metal atom is needed to dissociate methane. However, the exception was first noticed by Weaver et al. [107, 108] and later explained and corroborated trough x-ray diffraction experiments by Hellman et al. [10]. There is, in fact, a special site on oxidized palladium that is particularly active, namely PdO(101). Onto this site, methane adsorbs with an adsorption energy of 0.15 eV which is stronger than on any other surface (metallic or oxide) and the adsorption occurs with methane bridging the metal atom with two hydrogens. The adsorption of methane on to PdO(101) is enhanced by the electronic structure of Pd in the oxide, where the repulsion perceived by the molecule from the metals 5s states is reduced at this particular site. Moreover, the dissociation is aided by a hydrogen accepting oxygen atom on the surface. This example demonstrates how useful DFT is as a tool not only to obtain trends, but also to reveal mechanisms. Knowing the exact electronic requisites for enhanced surface reactivity is a prerequisite to design new catalytic materials.

There is another example of confusion between different studies when looking

at methane oxidation regarding the structural sensitivity of the reaction. Pd has both been measured to be structure sensitive [109] and independent of particle size [95]. Similar conflicting conclusions have been made for Pt [91, 110]. At the DFT level [46], there is no doubt that an enhanced reactivity is found on sites where the atom is under-coordinated: Final states energies are higher and activation barriers are lower (in a BEP manner).

There are other problems that affect the catalytic activity. One example is water, either being present as a product of methane conversion or added into the gas feed, which has an inhibiting effect on the rate, particularly for Pd. This has been throughly studied from an experimental point of view [92, 94, 96, 98, 111–114] but to our knowledge, never investigated through electronic structure calculations.

In contrast, the dissociation of methane over transition metals through electronic structure calculations, has been the object of numerous studies [89, 105, 115–120]. However, to be able to understand the entire reaction landscape and to use the information in a microkinetic study, adsorption of methane and adsorption energies of all its intermediates are needed. These calculations were done need calculated in Paper II.

6.2 Methane oxidation on Pd and Pt

The first part of the study was to create a reaction landscape for methane oxidation, from dissociation of CH_4 to combustion of the intermediates to water and CO_2. This was calculated for two planar surfaces (111), (100) and one stepped surface (211) for Pd and Pt. These calculations consider the reaction under rich conditions, with low oxygen content and no oxide formation. The second part was to identify possible reactions steps that could be rate limiting. In this case, the knowledge that water could be hindering to the reactions, made the inclusion of formation of water as a candidate to RDS, accompanied with the generally assumed limiting step, namely dissociative adsoption of methane. The third part was supply the DFT data into a microkinetic model.

The main conclusions of the study were that the reason behind the lack of agreement regarding the structure sensitivity of methane oxidation is due to that in spite of the higher reactivity of the step (with both higher adsorption energy and smaller activation barrier), the steps on both metals are poisoned by other adsorbates hindering methane dissociation. Hence, the reaction is in principle

structure sensitive, but smaller particles will not necessarily increase the rate of the reaction. Figure 6.1 shows calculated turnover frequencies as a function of temperature for the investigated facets. The facet with highest activity Pt(100). At low temperatures (under 450 K), the second most active facet is the Pt(111). The stepped site Pt(211) is less active due to hydroxyl poisoning on the surface. The Pd facets are generally less active than Pt, and follow the same trend, with Pd(100) having the highest rate, followed by the (111) and the step site is the less active surface under the investigated temperature range. The reason behind the low activity of Pd(211) is that the surface is oxygen poisoned.

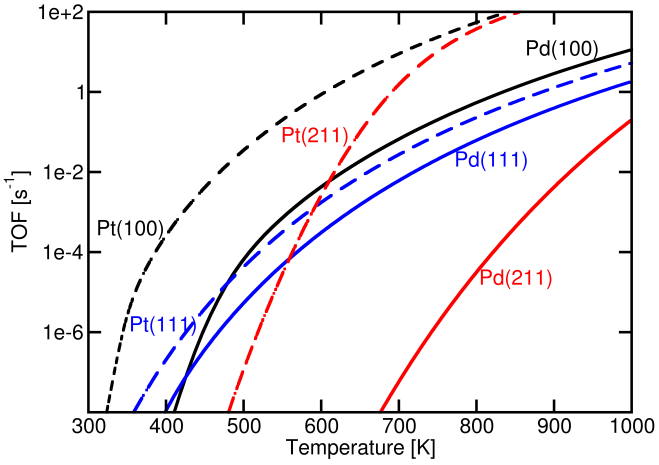

Figure 6.1: Turnover frequencies as a function of temperature for all the investigated facets.

The second conclusion is that the hindering of water, is not due to the fact that water formation is rate limiting, but due to the stability of adsorbed hydroxyls on the surface, which can be increased through hydrogen bonding.

Chapter 7

Conclusions and outlook

This chapter will try to discuss and summarize the most important conclusions of the present study also suggesting themes for for further studies.

7.1 General conclusions

The main objective of Paper I was to investigate the structure sensitivity of the bi-stability of CO oxidation over Pd and Pt. From the electronic structure calculations, it is clear that the activation barriers and adsorption energies change between different facets. The microkinetic simulations lead to the same conclusion: the activity of CO oxidation occurs at higher CO pressures on the (110) surface, followed by the (100). The surface with least reactivity is the (111) surface. Furthermore, the simulations show that the range of the bi-stability region is facet dependent, increasing with the reactivity of the facet. The comparison between Pd and Pt shows that the reason why Pd is more tolerant towards CO poisoning is the higher adsorption energies of oxygen atoms. The role of the sticking coefficient of oxygen is also of importance; the re-activation of the poisoned surface occurs at higher CO pressures on Pd as compared to Pt. These results are in excellent agreement with the experiments. The main conclusion is that the reactivity of each facet is directly related to the catalytic activity.

In Paper II, the focus was put on methane oxidation, where the reaction landscape has more elementary reaction steps and intermediate species. Also in this case, the DFT results reveal a clear structure sensitivity. The lowest activation energy for the dissociative adsorption of methane and the strongest adsorption energies on both Pd and Pt are calculated for the stepped surfaces. Furthermore, among the two metals, Pt has a more favorable reaction landscape, with lower

activation barriers, stronger adsorption energies and most favorable energetics. However, the results showed that the step will be poisoned by hydroxyl-groups or oxygen, hindering the oxidation of methane on these sites at experimental conditions. Hence, increasing the ratio of steps would not necessarily lead to higher catalytic activity. In summary for CO oxidation, higher reactivity of a facet leads to higher catalytic activity, for methane oxidation, the correlation is not clear. This could be due to the fact that the reaction landscape of methane oxidation involves many intermediate species that can affect the activity of the facet.

The methodology chosen in our reports is to perform comparisons between different systems. The papers show that activation barriers and adsorption energies are not always directly translatable to the activity of the catalyst. Including microkinetic modeling in the methodology provides a link between the micro and mesoscale shown in Figure 1.

7.2 Suggestions for future work

There are several steps that can be done to improve our understanding of the studied reactions. In paper II, methane oxidation was studied with a very simplistic reaction landscape. CH_4 was dissociated to elemental C and H and further oxidized. Obviously, the reaction landscape could be more elaborate with other competing pathways. For instance, oxygen could be introduced earlier in the reaction landscape, which would result in other intermediates like formaldehyde.

The second suggestion, also regarding methane oxidation, is the introduction of the oxide phases for Pd, and testing the model at lean conditions, with the inclusion of other reaction mechanisms reaction landscapes as the Mars van Krevelen pathway.

Another interesting study would be to investigate the oxidation of methane on clusters of 60 or more atoms, especially PdO clusters to seek for specially active sites, with an electronic structure that may resemble the one on the PdO(101) site.

Finally, the inclusion of the support would be helpful to understand the role of the support in the reactions, which in some cases seem to have a significant role for the activity.

Acknowledgments

This study would not have been possible without the financial support of Swedish Foundation for Strategic Research (SSF) within the project for Functionalized catalytic materials for demanding environment (FUNCAT).

The work was performed at the Competence Centre for Catalysis, which is hosted by Chalmers University of Technology and financially supported by the Swedish Energy Agency and the member companies: AB Volvo, ECAPS AB, Haldor Topsøe A/S, Saab Automobile Powertrain AB, Scania CV AB and Volvo Car Corporation AB.

The calculations have been performed at C3SE (Göteborg) and PDC (Stockholm) through a SNIC grant.

Henrik Grönbeck, my main supervisor: Thank you for helping me to learn and introducing me to the research field. For always being present and always having the door open. You are an example of dedication and love of science. I admire how you can approach a scientific task, both with meticulousness and creativity. Thank you for everything!

Anders Hellman, my assisting supervisor. Thank you for being an excellent teacher and introducing me to the field of computational physics. You are always fun to be around and you have the ability explain complicated problems in a simple way.

Magnus Skoglundh, thank you for the opportunity to work at KCK and for always providing of a warm and fun atmosphere.

Göran Whanström and **Lena Falk**, I thank you for all the help and guidance.

Per-Anders Carlsson, thank you for your experimental knowledge and insight on the catalysis. **Hanna Härelind**, thank you for being there.

Of course, a big thanks to all **coauthors** at the Technical University of Vienna, for a fruitful collaboration.

Ann, the secretary at TYK, thanks for all invaluable help regarding the ever so important small things.

Simon, **Jakub**, **Oliver** and **Maxim**: the computational team at KCK, we are a small group, but we do important stuff.

Oliver, my officemate. It feels like home in our little latino- jungle- paradise.

Everybody else at KCK, and Applied Surface Chemistry for the lovely atmosphere. In Particular, to **Hanna G.** you are a true friend, **Maria C.**, **Emma W.**, I miss you two! **Soran**, **Djamela**, **Sheedeh**, **Marika**, **Sasha**, **Freddy**, **Hannes**, **Emma A.**, **Linda**, **Björn**, **Johan**, **Jonathan**, **Alexander**, **Chlor**, **Ralph**, **Frida**, **Maria P.**, **Alberta**, **Markus**, **Christoffer**, **Romain**, **Ali**, **Adele**, **Matias**, **Moheb**, **Johanna** and all the others for the entertaining lunch and fika breaks.

To all the people in the group that I really belong to, namely Chemical Physics: I look forward to getting to know you better! Especially thanks to **Victoria**, **Carl**, **Anna**, **Björn**, **Cristoph**, **Fernando**, **Kristina**, **Beniamino**, **Pooya**, and all the others for all interesting discussion during the Monday fika.

Eva and **Göran**, **Johan** and **Anna**, my Swedish family, thank you!

My Mother, I have to thank you for everything!! Mostly, for showing me the world and for telling me how important it is to pursue your dreams. **My Father**, for showing me how important it is to love ones work, and for your dedication to your own field. My brothers **Juan**, **Mariano** and **Santiago**.

Simon, for all support, love, encouragement and understanding, but also for all the scientific discussions and collaboration between us.

Bibliography

[1] N. Künzli, R. Kaiser, S. Medina, M. Studnicka, O. Chanel, P. Filliger, M. Herry, F. H. Jr, V. Puybonnieux-Texier, P. Quenel, J. Schneider, R. Seethaler, J.-C. Vergnaud, and H. Sommer, *The Lancet*, vol. 356, p. 795, 2000.

[2] I. Chorkendorff and J. W. Niemantsverdriet, *Concepts of Modern Catalysis and Kinetics*. Wiley-VCH, 2003.

[3] V. Pârvulescu, P. Grange, and B. Delmon, *Catal. Today*, vol. 46, p. 233, 1998.

[4] L. D. Prockop and R. I. Chichkova, *J. Neurol. Sci.*, vol. 262, p. 122, 2007.

[5] R. M. Heck and R. J. Farrauto, *App. Catal. A*, vol. 221, p. 443, 2001.

[6] F. Tao, M. E. Grass, Y. Zhang, D. R. Butcher, J. R. Renzas, Z. Liu, J. Y. Chung, B. S. Mun, M. Salmeron, and G. A. Somorjai, *Science*, vol. 322, p. 932, 2008.

[7] G. Ertl, *Science*, vol. 254, p. 1750, 1991.

[8] K. H. Hansen, T. Worren, S. Stempel, E. Lægsgaard, M. Bäumer, H.-J. Freund, F. Besenbacher, and I. Stensgaard, *Phys. Rev. Lett.*, vol. 83, p. 4120, 1999.

[9] F. Besenbacher, E. L. , and I. Stensgaard, *Mat. Today*, vol. 8, p. 26, 2005.

[10] A. Hellman, A. Resta, N. M. Martin, J. Gustafson, A. Trinchero, P.-A. Carlsson, O. Balmes, R. Felici, R. van Rijn, J. W. M. Frenken, J. N. Andersen, E. Lundgren, and H. Grönbeck, *J. Phys. Chem. Lett.*, vol. 3, p. 678, 2012.

[11] H. G. E. Becker, P. A. Carlsson and M. Skoglundh, *J. Catal.*, vol. 252, p. 11, 2007.

[12] J. Libuda and H.-J. Freund, *Surf. Sci. Rep.*, vol. 57, p. 157, 2005.

[13] H.-J. Freund, M. Bäumer, J. Libuda, T. Risse, G. Rupprechter, and S. Shaikhutdinov, *J. Catal.*, vol. 216, p. 223, 2003.

[14] R. Schlögl, *CATTECH*, vol. 5, p. 146, 2001.

[15] P. Broqvist, Ph.D. dissertation, Chalmers University of Technology, 2005.

[16] R. W. Bentley, S. A. Mannan, and S. J. Wheeler, *Energy Policy*, vol. 35, p. 6364, 2007.

[17] P. de Almeida and P. D. Silva, *Energy Policy*, vol. 37, p. 1267, 2009.

[18] G. W. Huber, S. Iborra, and A. Corma, *Chem. Rev.*, vol. 106, p. 4044, 2006.

[19] B. Kasemo, H. Frank, S. Kullander, M. Lindgren, T. Malmer, C. Sjöding, and E. Stattin, *En bok om energi från IVA och KVA*. Kungliga ingenjörsvetenskapakademin, 2007.

[20] http://www.ngvjournal.dreamhosters.com/en/statistics/item/911-worldwide-ngv-statistics (15-03-13).

[21] P. Gelin and M. Primet, *Appl. Catal. B*, vol. 39, p. 1, 2002.

[22] D. A. Lashof and D. R. Ahuja, *Lett. Nature*, vol. 344, p. 529, 1990.

[23] D. S. Lafyatis, G. P. Ansell, S. C. Bennett, J. C. Frost, P. J. Millington, R. R. Rajaram, A. P. Walker, and T. H. Ballinger, *App. Catal. B*, vol. 18, p. 123, 1998.

[24] R. Imbihl and G. Ertl, *Chem. Rev.*, vol. 95, p. 697, 1995.

[25] C. T. Campbell, G. Ertl, H. Kuipers, and J. Segner, *J. Chem. Phys.*, vol. 73, p. 5862, 1980.

[26] M. Ehsasi, M. Berdau, T. Rebitzki, K.-P. Charle, K. Christmann, and J. H. Block, *J. Chem. Phys.*, vol. 98, p. 9177, 1993.

[27] J. Szany and W. D. Goodman, *J. Phys. Chem.*, vol. 98, p. 2972, 1994.

[28] A. Hellman, S. Klacar, and H. Grönbeck, *J. Am. Chem. Soc.*, vol. 131, p. 16636, 2009.

[29] F. Abild-Pedersen and M. Andersson, *Surf. Sci.*, vol. 601, p. 1747, 2007.

[30] A. Eichler, *Surf. Sci.*, vol. 498, p. 314, 2002.

[31] M. Berdau, G. G. Yelenin, A. Karpowicz, M. Ehsasi, K. Christmann, and J. H. Block, *J. Chem. Phys.*, vol. 110, p. 11551, 1999.

[32] H. Falsig, B. H. I. S. Kristensen, T. J. T. Bligaard, C. H. Christensen, and J. K. Nørskov, *Angew. Chem. Int. Ed.*, vol. 47, p. 4835, 2008.

[33] P. J. Feibelman, B. Hammer, J. K. Nørskov, F. Wagner, M. Scheffler, R. Stumpf, R. Watwe, and J. Dumesic, *J. Phys. Chem. B*, vol. 105, p. 4018, 2001.

[34] S. Yamagishi, T. Fujimoto, Y. Inada, and H. Orita, *J. Phys. Chem. B*, vol. 109, p. 8899, 2005.

[35] C. J. Zhang and P. Hu, *J. Am. Chem. Soc.*, vol. 123, p. 1166, 2001.

[36] P. Atkins and J. de Paula, *Physical Chemistry, 8th Ed.* Oxford University Press, 2006.

[37] J. I. Gersten and F. W. Smith, *The Physics and Chemistry of Materials.* John Wiley & sons, 2001.

[38] C. Herring, *Phys. Rev.*, vol. 82, p. 87, 1951.

[39] L. Vitos, A. V. Ruban, H. L. Skriver, and J. Kollar, *Surf. Sci.*, vol. 411, p. 186, 1998.

[40] P. L. Hansen, J. B. Wagner, S. Helveg, J. R. Rostrup-Nielsen, B. S. Clausen, and H. Topsøe, *Science*, vol. 295, p. 2053, 2002.

[41] P. D. Nolan, B. R. Lutz, P. L. Tanaka, J. E. Davis, and C. B. Mullins, *J. Chem. Phys.*, vol. 111, p. 3696, 1999.

[42] B. Hammer and J. K. Nørskov, ser. Adv. Catal. Academic Press, 2000, vol. 45, p. 71.

[43] D. M. Newns, *Phys. Rev.*, vol. 178, p. 1123, 1969.

[44] P. W. Anderson, *Phys. Rev.*, vol. 124, p. 41, 1961.

[45] B. Hammer and J. K. Nørskov, *Nature*, vol. 376, p. 238, 2002.

[46] B. Hammer and J. K. Nørskov, *Surf. Sci.*, vol. 343, p. 211, 1995.

[47] B. Hammer and J. K. Nørskov, *Nature*, vol. 376, p. 238, 2002.

[48] G. Blyholder, *J. Phys. Chem.*, vol. 68, p. 2772, 1964.

[49] J. N. Brønsted, *Chem. Rev.*, vol. 5, p. 231, 1928.

[50] M. G. Evans and M. Polanyi, *Trans. Faraday Soc.*, vol. 34, p. 11, 1938.

[51] J. K. Nørskov, T. Bligaard, A. Logadottir, S. Bahn, L. Hansen, M. Bollinger, H. Bengaard, B. Hammer, Z. Sljivancanin, M. Mavrikakis, Y. Xu, S. Dahl, and C. Jacobsen, *J. Catal.*, vol. 209, p. 275, 2002.

[52] T. Bligaard, J. Nørskov, S. Dahl, J. Matthiesen, C. Christensen, and J. Sehested, *J. Catal.*, vol. 224, p. 206, 2004.

[53] W. Kotch and M. C. Holthausen, *A Chemist's Guide to Density Functional Theory.* Wiley-VCH, 2008.

[54] R. M. Martin, *Electronic Structure.* Cambridge University Press, 2010.

[55] A. Szabo and N. S. Ostlund, *Modern Quantum Chemistry.* Dover Publications, INC, 1996.

[56] E. Schrödinger, *Phys. Rev.*, vol. 28, p. 1049, 1926.

[57] D. R. Hartree, *Mathematical Proceedings of the Cambridge Philosophical Soc.*, vol. 24, p. 89, 1928.

[58] D. R. Hartree, *Mathematical Proceedings of the Cambridge Philosophical Soc.*, vol. 24, p. 111, 1928.

[59] D. R. Hartree, *Mathematical Proceedings of the Cambridge Philosophical Soc.*, vol. 24, p. 426, 1928.

[60] J. C. Slater, *Phys. Rev.*, vol. 32, p. 339, 1928.

[61] V. Fock, *Zeitschrift für Physik*, vol. 61, p. 126, 1930.

[62] W. Kohn and L. J. Sham, *Phys. Rev.*, vol. 140, p. A1133, 1965.

[63] R. O. Jones and O. Gunnarsson, *Rev. Mod. Phys.*, vol. 61, p. 689, 1989.

[64] J. P. Perdew and K. Schmidt, *AIP Conference Proceedings*, vol. 577, p. 1, 2001.

[65] J. C. Slater, *Phys. Rev.*, vol. 81, p. 385, 1951.

[66] D. M. Ceperley and B. J. Alder, *Phys. Rev. Lett.*, vol. 45, p. 566, 1980.

[67] S. H. Vosko, L. Wilk, and M. M. Nusair, *Can. J. Phys.*, vol. 58, p. 1200, 1980.

[68] M. Körling and J. Häglund, *Phys. Rev. B*, vol. 45, p. 13293, 1992.

[69] J. P. Perdew, K. Burke, and M. Ernzerhof, *Phys. Rev. Lett.*, vol. 77, p. 3865, 1996.

[70] J. Wellendorff, "Versatile density functional for computational surface science," Ph.D. dissertation, Technical University of Denmark, 2012.

[71] J. J. Mortensen, L. B. Hansen, and K. W. Jacobsen, *Phys. Rev. B*, vol. 71, p. 035109, 2005.

[72] P.-A. Carlsson, M. Skoglundh, P. Thormählen, and B. Andersson, *Top. Catal.*, vol. 30-31, p. 375, 2004.

[73] P.-A. Carlsson, V. P. Zhdanov, and B. Kasemo, *App. Surf. Sci.*, vol. 239, p. 424, 2005.

[74] D. McQuarrie and J. D. Simon, *Molecular Thermodynamics*. University Sci. Books, 1999.

[75] G. Mills and H. Jónsson, *Phys. Rev. Lett.*, vol. 72, p. 1124, 1994.

[76] T. A. Halgren and W. N. Lipscomb, "The synchronous-transit method for determining reaction pathways and locating molecular transition states," *Chem. Phys. Lett.*, vol. 49, p. 225, 1977.

[77] M. Ehsasi, M. Berdau, T. Rebitzki, K.-P. Charle, K. Christmann, and J. H. Block, *J. Chem. Phys.*, vol. 98, p. 9177, 1993.

[78] M. D. Graham, I. G. Kevrekidis, K. Asakura, J. Lauterbach, K. Krischer, H.-H. Rotermund, and G. Ertl, *Science*, vol. 264, p. 80, 1994.

[79] M. Kim, M. Bertrams, M. Pollmann, A. von Oertzen, A. S. Mikhailov, H. H. Rotermund, and G. Ertl, *Sci.*, vol. 292, p. 1357, 2001.

[80] P. Salo, K. Honkala, M. Alatalo, and K. Laasonen, *Surf. Sci.*, vol. 516, p. 247, 2002.

[81] J. Rogal, K. Reuter, and M. Scheffler, *Phys. Rev. B*, vol. 75, p. 205433, 2007.

[82] M. Skoglundh and E. Fridell, *Topics in Catal.*, vol. 28, p. 79, 2004.

[83] G. Rupprechter, T. Dellwig, H. Unterhalt, and H.-J. Freund, *J. Phys. Chem. B*, vol. 105, p. 3797, 2001.

[84] W. A. Brown, R. Kose, and D. A. King, *Chem. Rev.*, vol. 98, p. 797, 1998.

[85] V. Zhdanov and B. Kasemo, *Surf. Sci. Rep.*, vol. 20, p. 113, 1994.

[86] S. Johansson, L. Österlund, and B. Kasemo, *J. Catal.*, vol. 201, p. 275, 2001.

[87] M. Aryafar and F. Zaera, *Catal. Lett.*, vol. 48, p. 173, 1997.

[88] J. Han, D. Y. Zemlyanov, and F. H. Ribeiro, *Catal. Today*, vol. 117, p. 506, 2006.

[89] A. T. Anghel, D. J. Wales, S. J. Jenkins, and D. A. King, *Phys. Rev. B*, vol. 71, p. 113410, 2005.

[90] E. Becker, P.-A. Carlsson, and M. Skoglundh, *Top. Catal.*, vol. 52, p. 1957, 2009.

[91] R. Burch and P. K. Loader, *Appl. Catal. B*, vol. 5, p. 149, 1994.

[92] R. Burch, F. J. Urbano, and P. K. Loader, *Appl. Catal. A*, vol. 123, p. 173, 1995.

[93] P.-A. Carlsson and M. Skoglundh, *Appl. Catal. B*, vol. 101, p. 669, 2011.

[94] D. Ciuparu and L. Pfefferle, *App. Catal. A*, vol. 209, p. 415, 2001.

[95] C. F. Cullis and B. M. Willatt, *J. Catal.*, vol. 83, p. 267, 1983.

[96] C. F. Cullis, T. G. Nevell, and D. L. Trimm, *Faraday Trans.*, vol. 1, pp. 1406–1412, 1972.

[97] J. G. McCarty, *Catal. Today*, vol. 26, p. 283, 1995.

[98] F. H. Ribeiro, M. Chow, and R. A. Dallabetta, *J. Catal.*, vol. 146, p. 537, 1994.

[99] R. J. Farrauto, J. K. Lampert, M. C. Hobson, and E. M. Waterman, *App. Catal. B*, vol. 6, p. 263, 1995.

[100] R. Burch, *Pure Appl. Chem.*, vol. 68, p. 377, 1996.

[101] R. Burch, *Catal. Today*, vol. 35, p. 27, 1997.

[102] C. A. Müller, M. Maciejewski, R. A. Koeppel, and A. Baiker, *J. Catal.*, vol. 166, p. 36, 1997.

[103] S. C. Su, J. N. Carstens, and A. T. Bell, *J. Catal.*, vol. 176, p. 125, 1998.

[104] J. N. Carstens, S. C. Su, and A. T. Bell, *J. Catal.*, vol. 176, p. 136, 1998.

[105] C.-Q. Lv, K.-C. Ling, and G.-C. Wang, *J. Chem. Phys.*, vol. 131, p. 144704, 2009.

[106] M. Blanco-Rey and S. J. Jenkins, *J. Chem. Phys.*, vol. 130, p. 014705, 2009.

[107] J. F. Weaver, C. Hakanoglu, A. Antony, and A. Asthagiri, *J. Am. Chem. Soc.*, vol. 133, p. 16196, 2011.

[108] J. F. Weaver, C. Hakanoglu, J. M. Hawkins, and A. Asthagiri, *J. Chem. Phys.*, vol. 132, p. 024709, 2010.

[109] R. F. Hicks, H. Qi, M. L. Young, and R. Lee, *J. Catal.*, vol. 122, p. 280, 1990.

[110] K. Otto, *Langmuir*, vol. 5, p. 1364, 1989.

[111] C. F. Cullis and B. M. Willatt, *J. Catal.*, vol. 86, p. 187, 1984.

[112] J. van Giezen, F. van den Berg, J. Kleinen, A. van Dillen, and J. Geus, *Catal. Today*, vol. 47, p. 287, 1999.

[113] D. Ciuparu, N. Katsikis, and L. Pfefferle, *App. Catal. A*, vol. 216, p. 209, 2001.

[114] P. Gelin, L. Urfels, M. Primet, and E. Tena, *Catal. Today*, vol. 83, p. 45, 2003.

[115] S. Nave and B. Jackson, *J. Chem. Phys.*, vol. 130, p. 054701, 2009.

[116] S. Nave, A. K. Tiwari, and B. Jackson, *J. Chem. Phys.*, vol. 132, p. 054705, 2010.

[117] W. An, X. C. Zeng, and C. H. Turner, *J. Chem. Phys.*, vol. 131, p. 174702, 2009.

[118] C. J. Zhang and P. Hu, *J. Chem. Phys.*, vol. 116, p. 322, 2002.

[119] R. M. Watwe, H. S. Bengaard, J. R. Rostrup-Nielsen, J. A. Dumesic, and J. K. N, *J. Catal.*, vol. 189, p. 16, 2000.

[120] B. Xing, X.-Y. Pang, G.-C. Wang, and Z.-F. Shang, *J. Mol. Catal. A*, vol. 315, p. 187, 2010.